

The Energy Decay of Warm-core Eddies in the Gulf of Mexico

Thomas Meunier¹, Amy S Bower¹, Paula Pérez-Brunius², and Federico Graef³

¹Woods Hole Oceanographic Institution

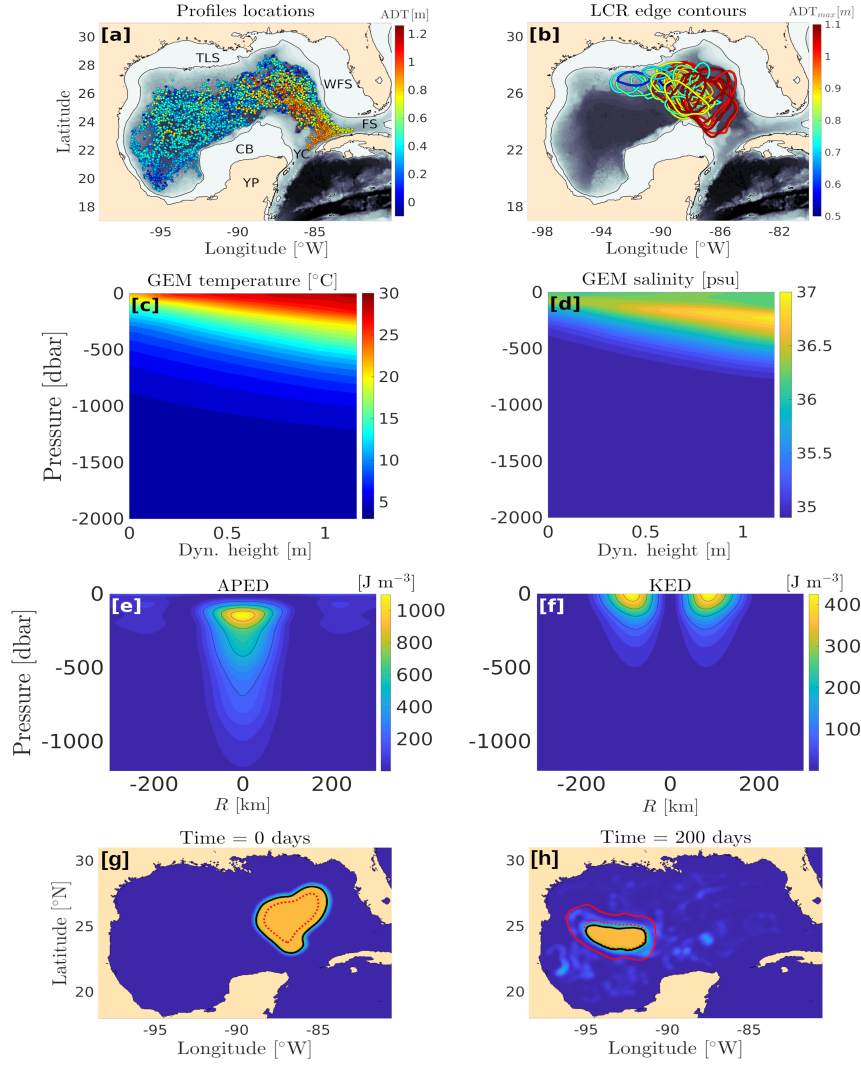
²Ensenada Center for Scientific Research and Higher Education

³CICESE

October 17, 2023

Abstract

The Gulf of Mexico (GoM) is home to some of the most energetic eddies in the ocean. They detach from the Loop-Current and drift through the basin, transporting large amounts of heat and salt. These eddies, known as Loop Current rings (LCRs) have a crucial role in the GoM's dynamics and in the weather of the eastern US, and this role is largely conditioned by their longevity and decay properties. Here, we use an empirical method to estimate the energy evolution of all LCRs detached since 1993. We found that, contrary to the commonly accepted idea that LCRs conserve their energy as they drift through the GoM and decay suddenly against the western platform, LCRs' energy decays faster in the eastern basin, and they typically lose three-quarter of their energy before encountering the continental shelf. We also show that wind-current feedback largely contributes to the energy decay and conversion.



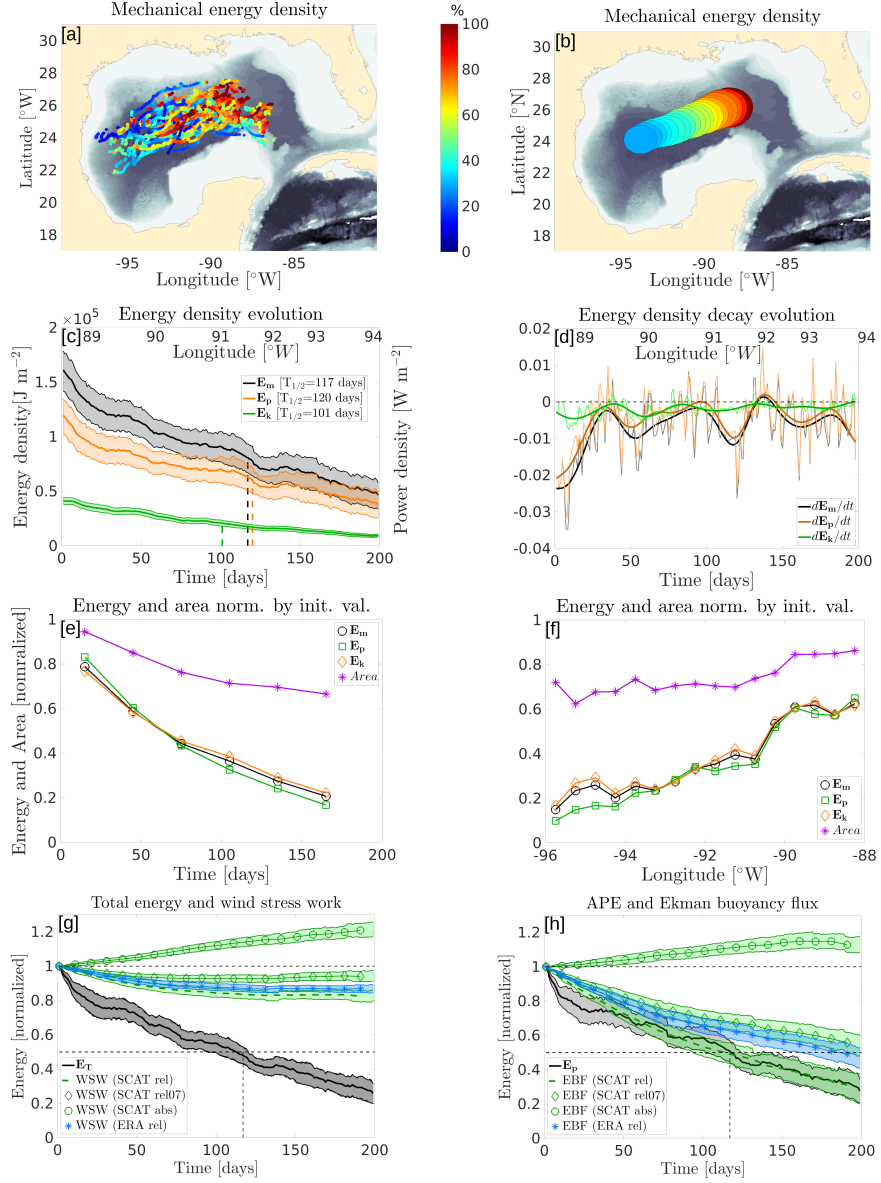
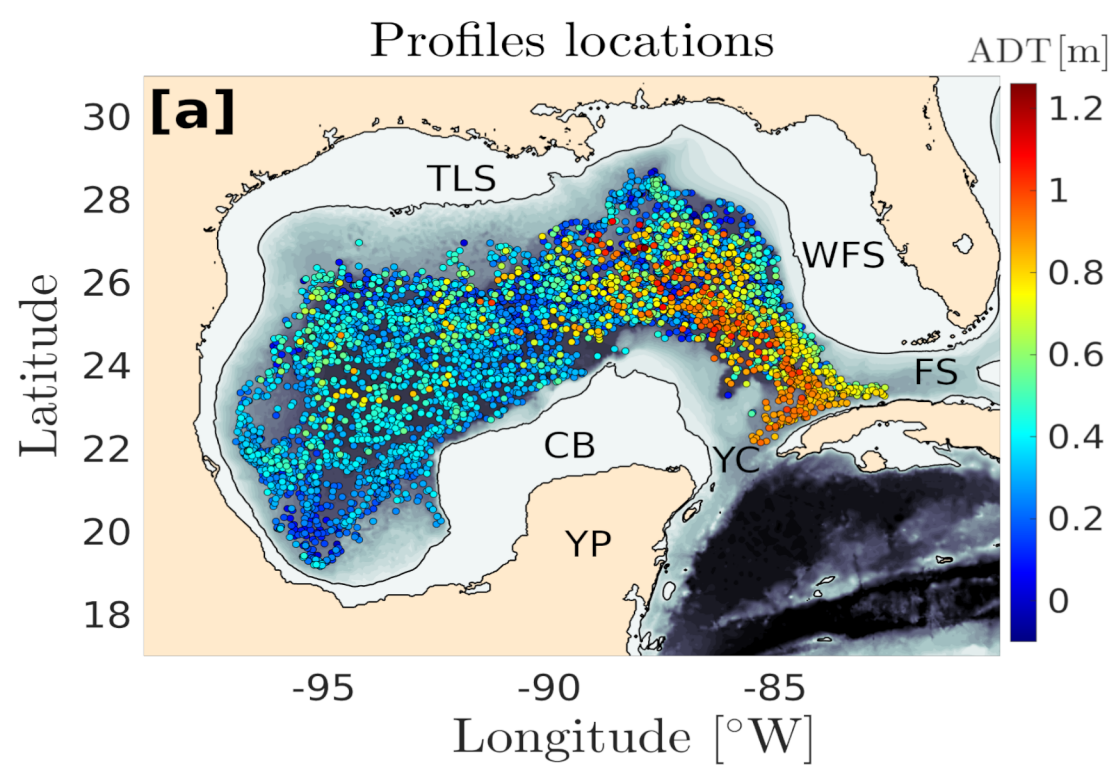
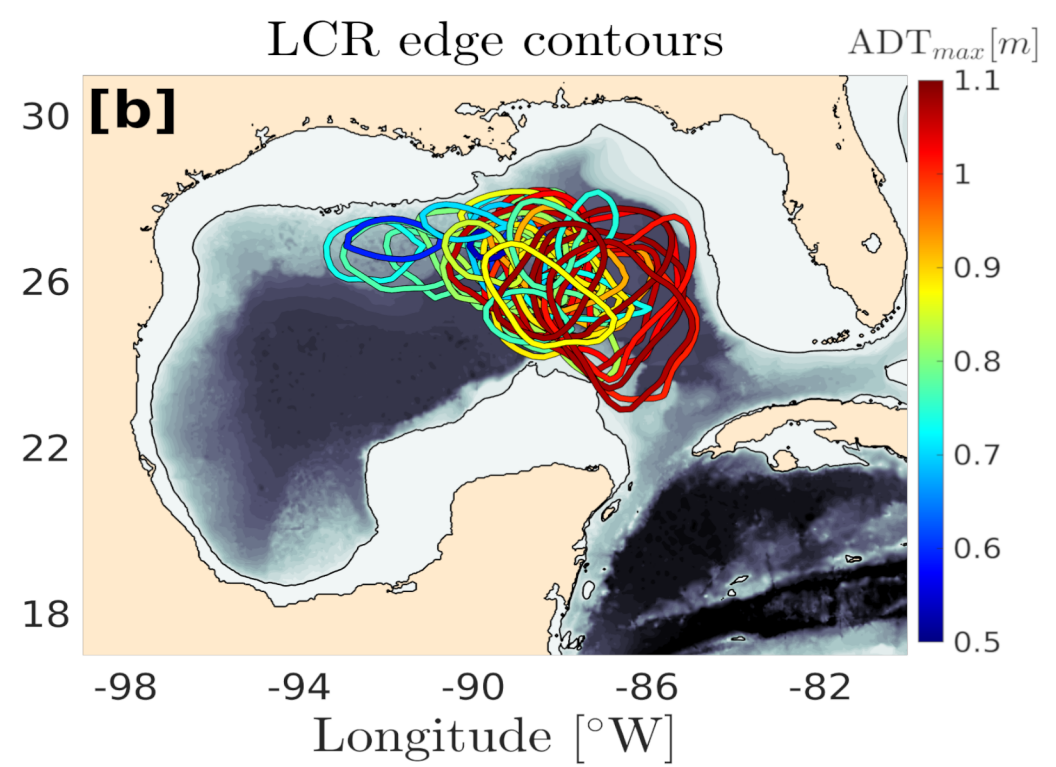
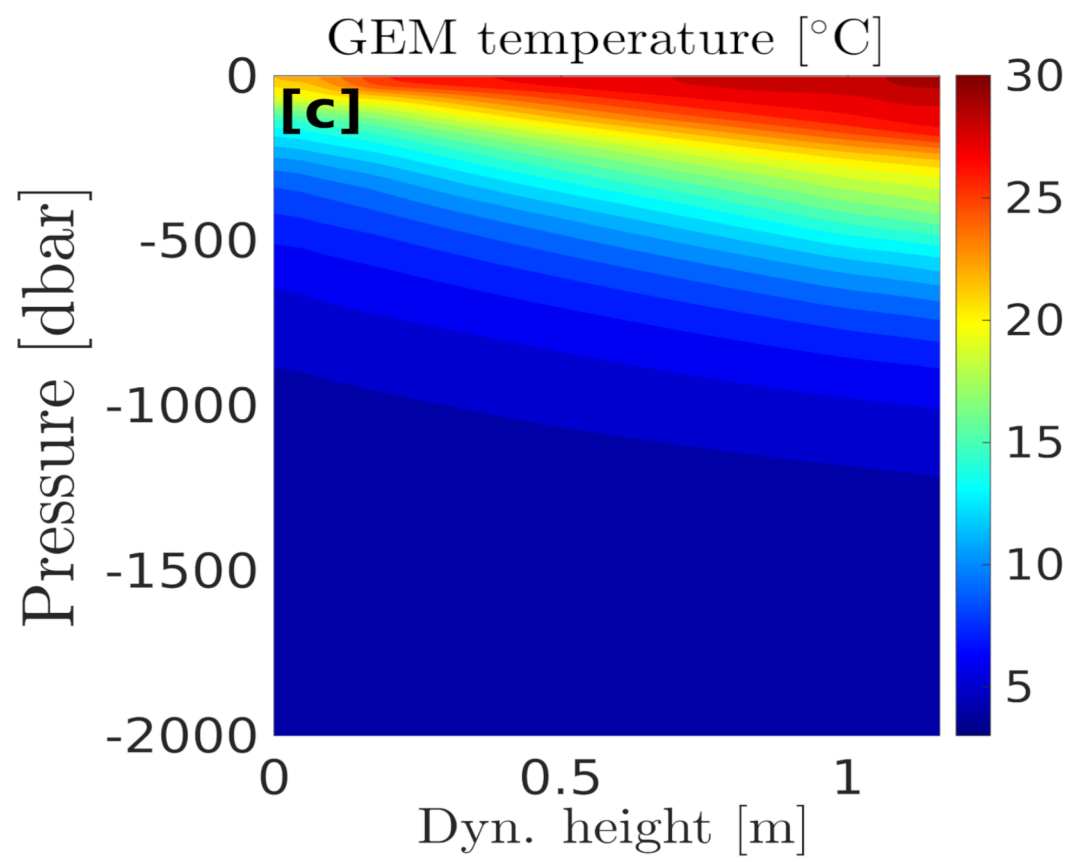


Figure 1.

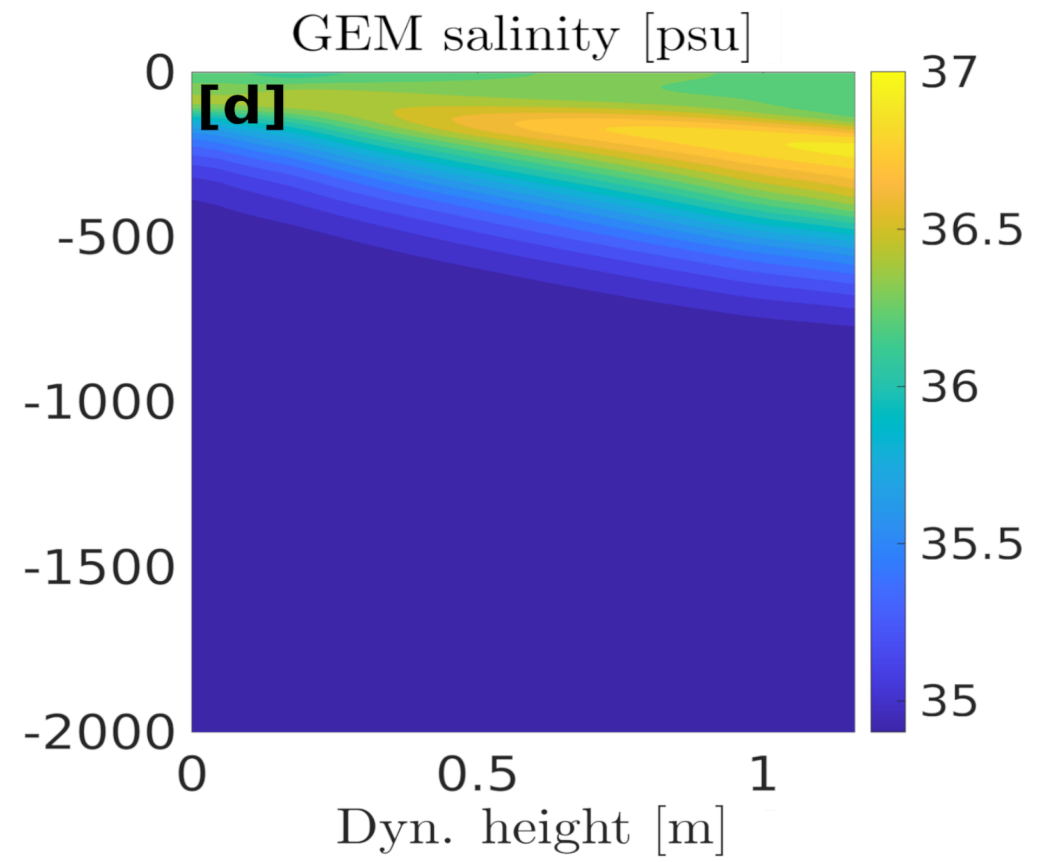
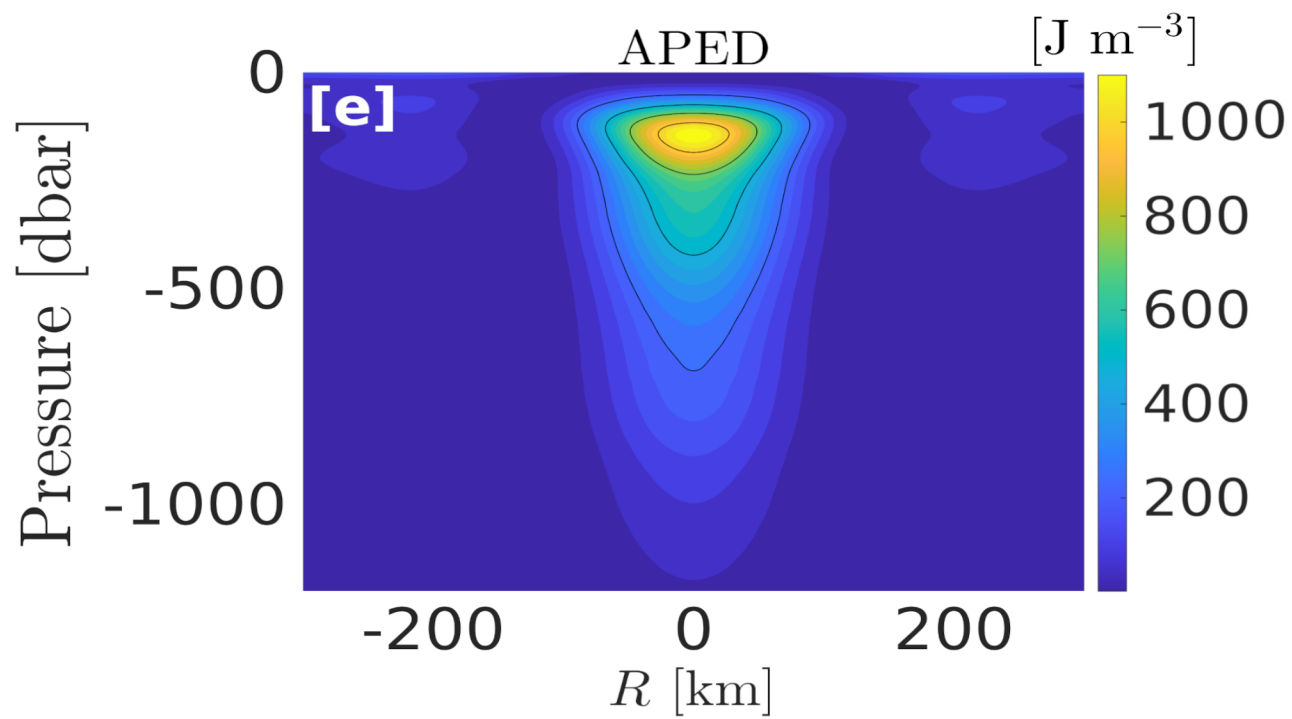
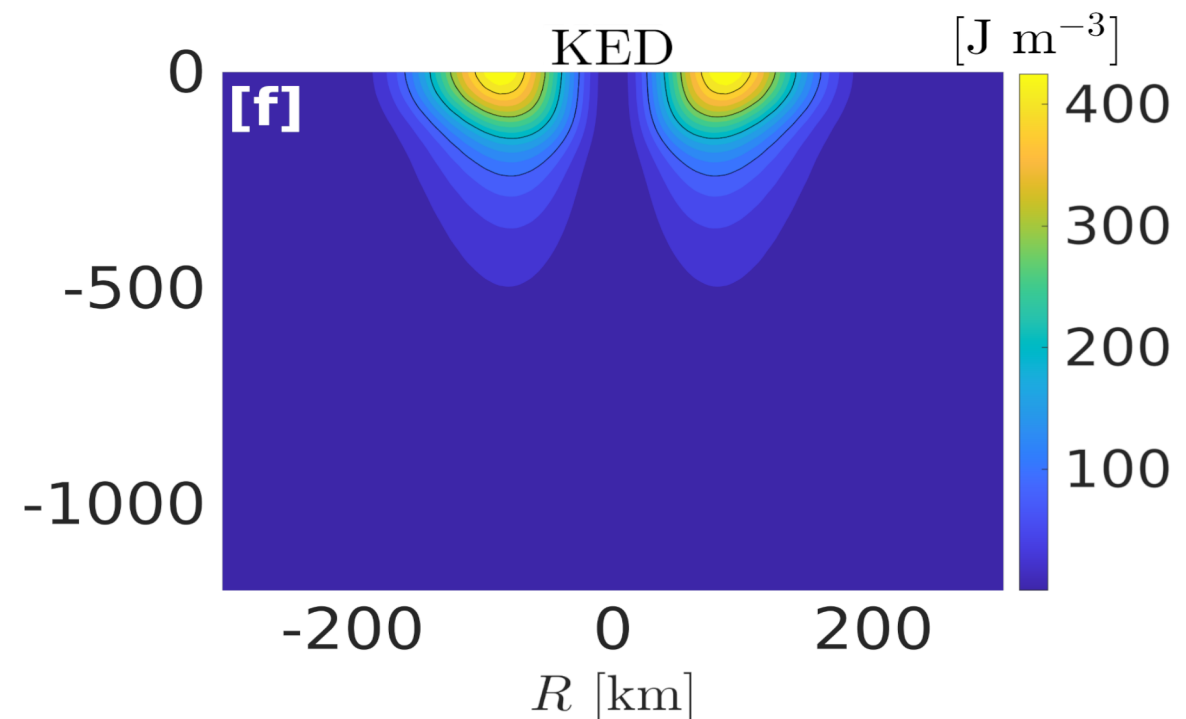
Profiles locations



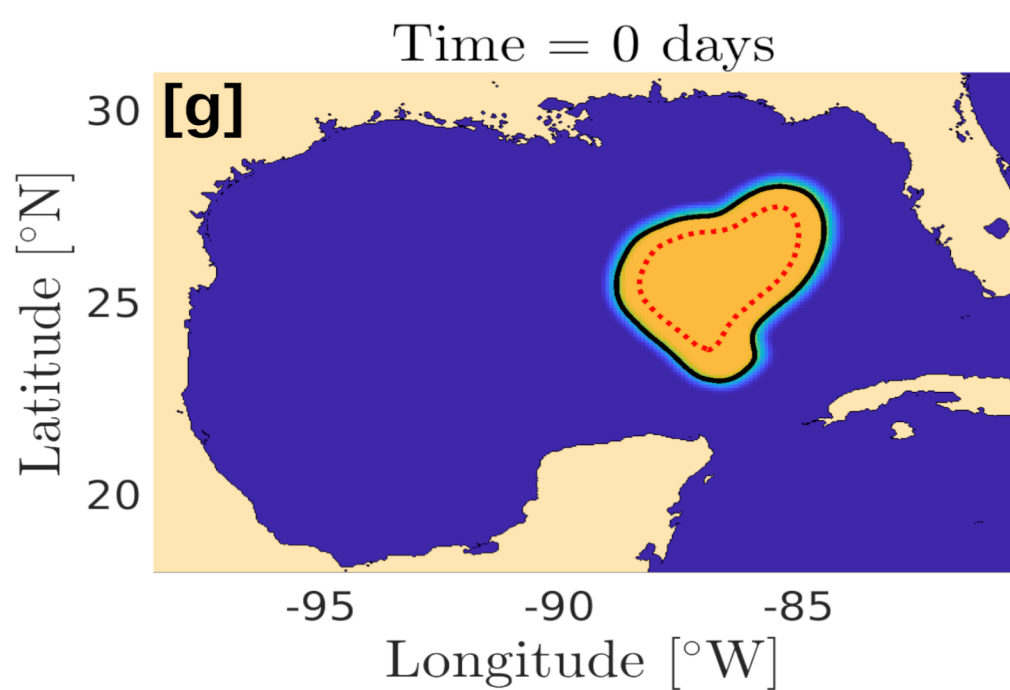
LCR edge contours

GEM temperature [$^{\circ}$ C]

GEM salinity [psu]

APED [J m^{-3}]KED [J m^{-3}]

Time = 0 days



Time = 200 days

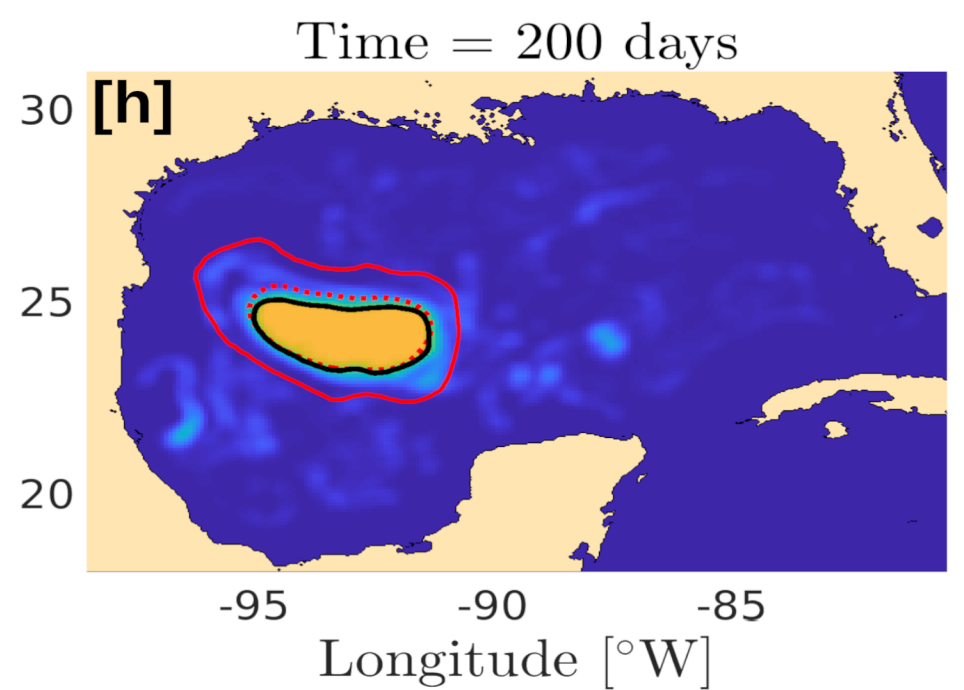
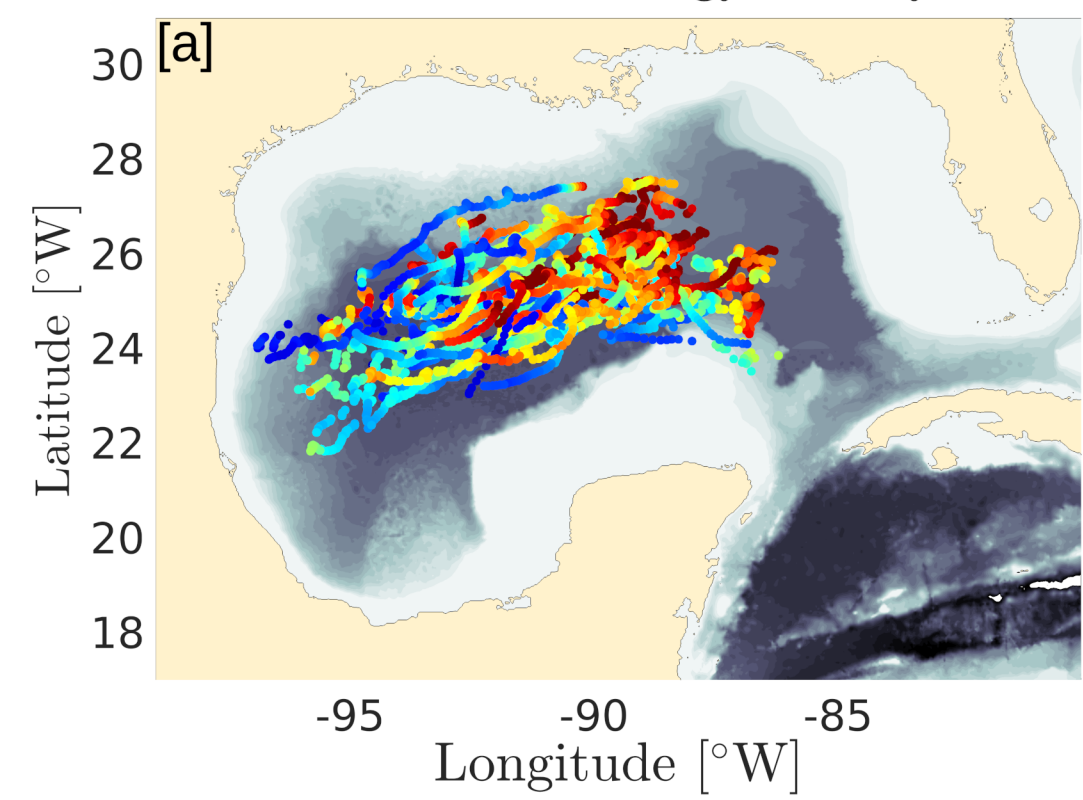
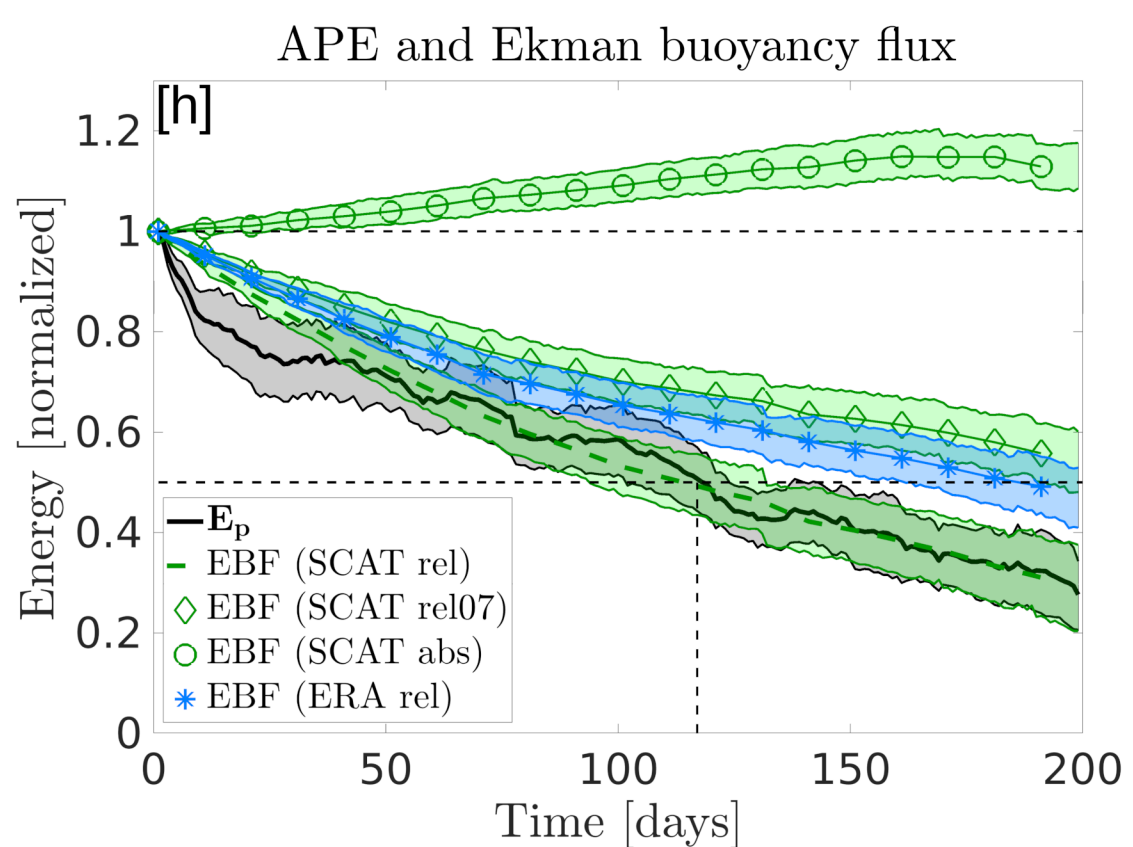
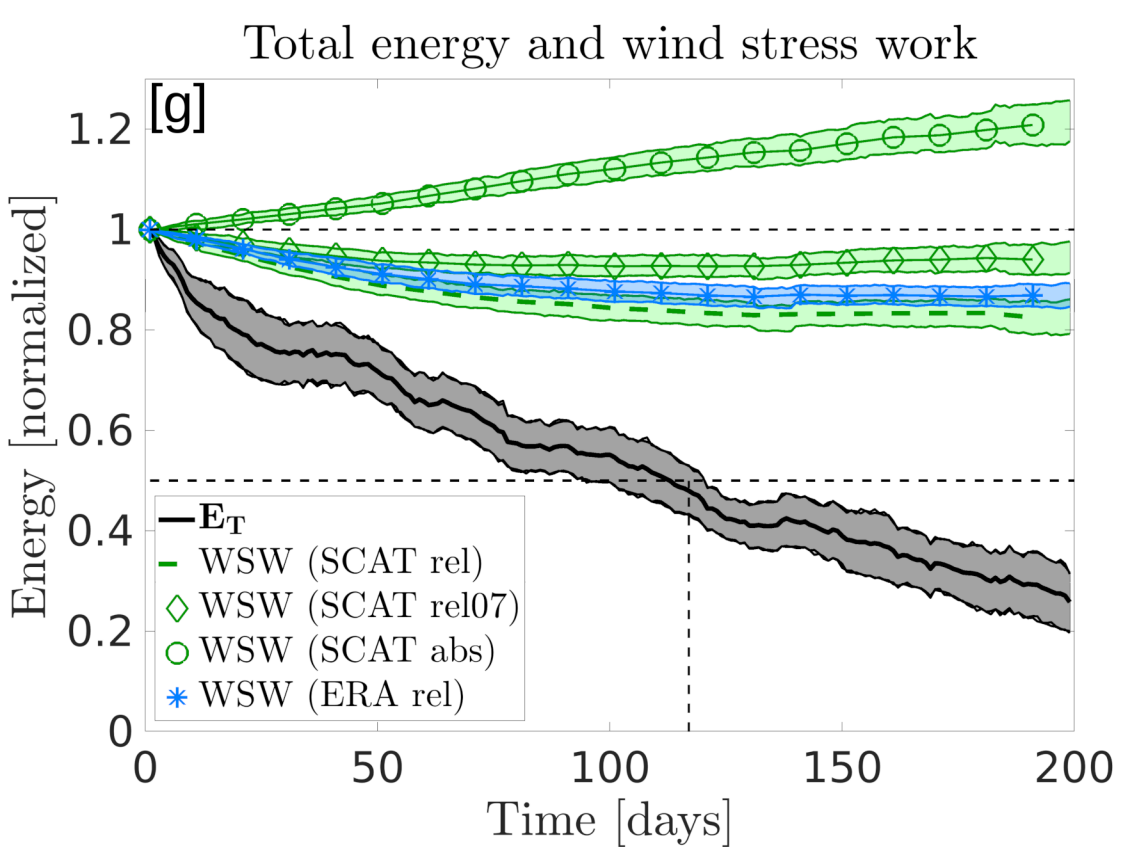
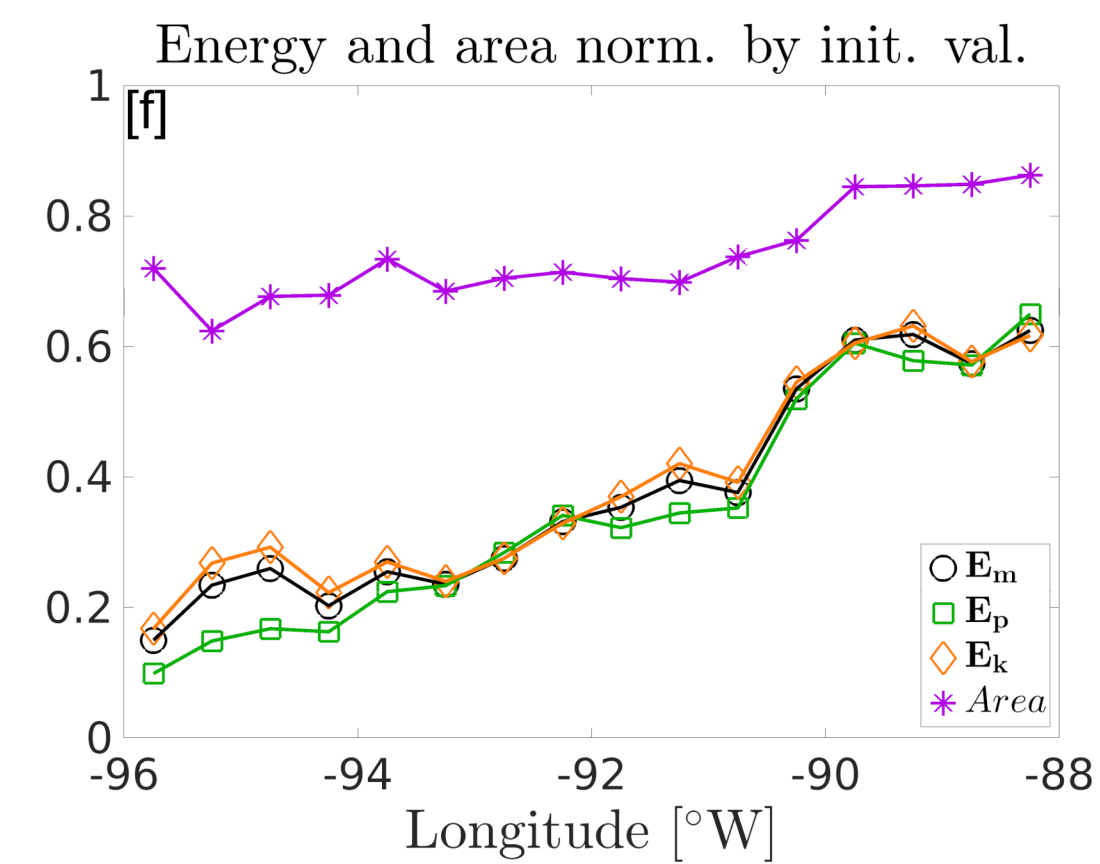
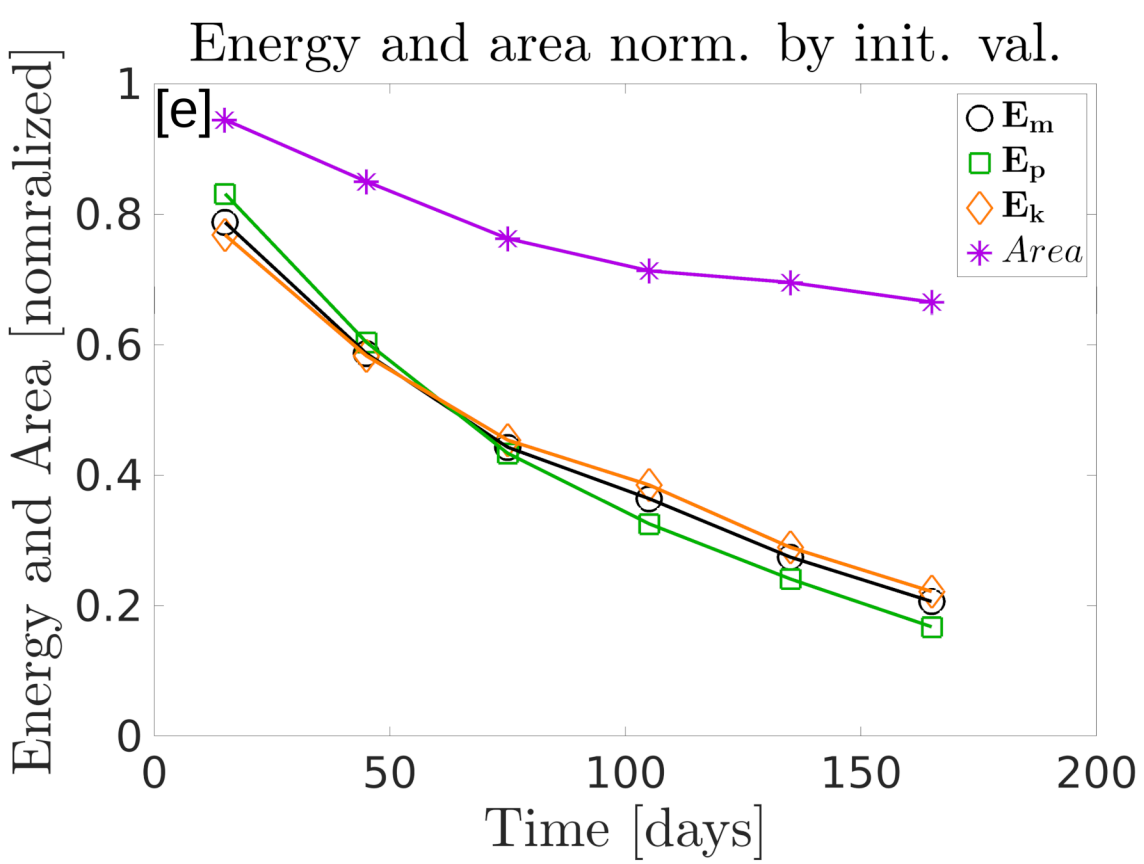
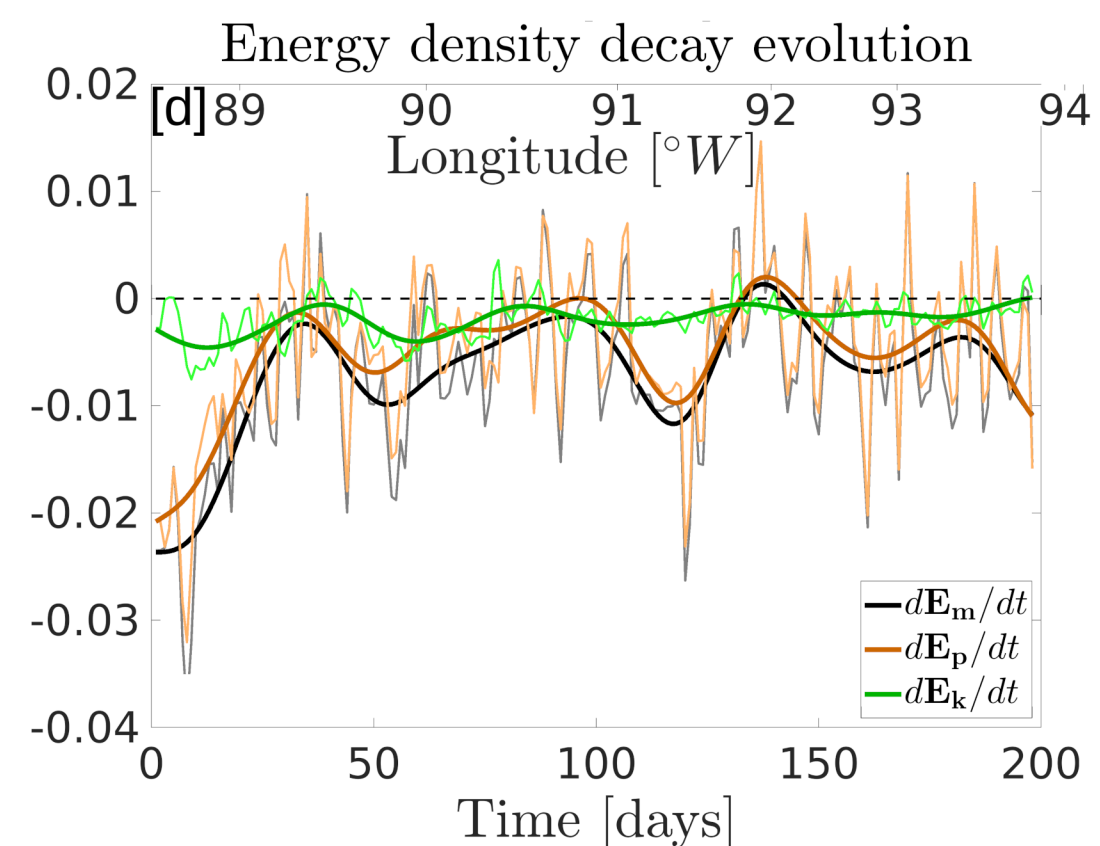
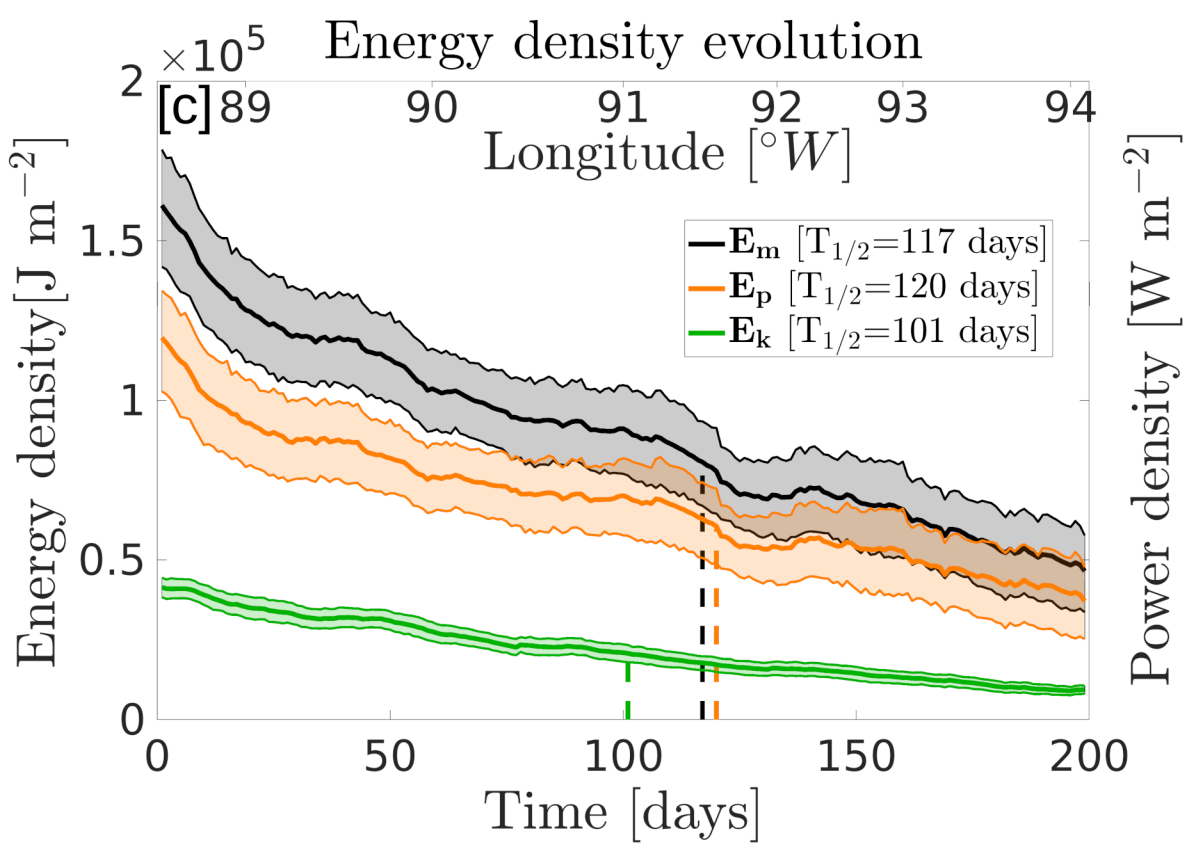
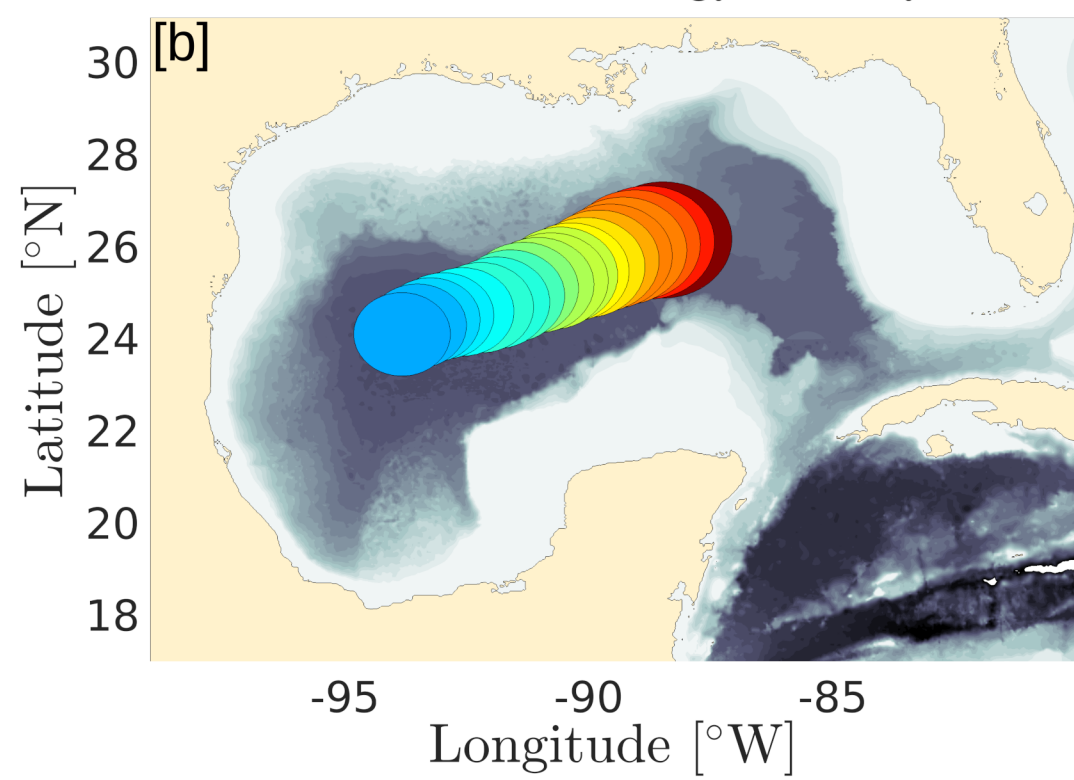


Figure 2.

Mechanical energy density



Mechanical energy density



1 **The Energy Decay of Warm-core Eddies in the Gulf of**
2 **Mexico**

3 **Thomas Meunier¹, Amy Bower¹, Paula Pérez-Brunius², and Federico Graef²**

4 ¹Woods Hole Oceanographic Institution, 360 Woods Hole road, Woods Hole, MA02543, USA

5 ²CICESE, Carretera Ensenada-Tijuana 3918, Ensenada BC 22860, Mexico

6 **Key Points:**

- 7 • Time evolution of the energy of Warm-core rings in the Gulf of Mexico is assessed
8 using empirical methods and satellite altimetry.
9 • The vast majority of mechanical energy (kinetic plus available potential) is lost
10 early in the eddies life cycles, far from the western boundary.
11 • Wind-current feed back effects such as Ekman buoyancy flux and wind stress work
12 play an important role in energy conversion and decay.

Abstract

The Gulf of Mexico (GoM) is home to some of the most energetic eddies in the ocean. They detach from the Loop-Current and drift through the basin, transporting large amounts of heat and salt. These eddies, known as Loop Current rings (LCRs) have a crucial role in the GoM's dynamics and in the weather of the eastern US, and this role is largely conditioned by their longevity and decay properties. Here, we use an empirical method to estimate the energy evolution of all LCRs detached since 1993. We found that, contrary to the commonly accepted idea that LCRs conserve their energy as they drift through the GoM and decay suddenly against the western platform, LCRs' energy decays faster in the eastern basin, and they typically lose three-quarter of their energy before encountering the continental shelf. We also show that wind-current feedback largely contributes to the energy decay and conversion.

Plain Language Summary

Ocean eddies can be long-lived and carry large amounts of heat and salt across ocean basins and marginal seas. This is the case of Loop Current rings (LCRs), which are large warm-core eddies drifting through the Gulf of Mexico (GoM). Understanding how these eddies lose their energy is key to understand their longevity and transport properties. Here, we use a previously validated empirical method based on *in situ* observations to estimate the time evolution of LCRs energy using satellite observations. We show that LCRs decay continuously during their life cycle, contrary to the previously accepted idea that they decay when collapsing against the western GoM's continental shelf. LCRs have already lost three-quarter of their energy before they reach any topographic obstacle. Using wind observations, we also show that wind-current interactions are key to the energy loss of these eddies.

1 Introduction

Coherent eddies can carry tracers across oceanic basins and participate in the transport of water-masses that impact large scale circulation and climate as well as ecosystems. For instance, Loop Current rings (LCRs), detaching from the Loop Current (LC), carry warm subtropical underwater (SUW) originating from the Caribbean through the Gulf of Mexico (Elliott, 1982; Leben, 2005) and have a direct impact on the basin's water mass properties (Vidal et al., 1994; Hamilton et al., 2018; T. Meunier et al., 2020), hurricane intensification (Shay et al., 2000; Jaimes et al., 2016), and thunderstorm occurrence east of the Rocky mountains (Molina et al., 2016). Similarly, Agulhas rings carry anomalously warm and salty Indian Ocean water through the South Atlantic and participate in the upper limb of the Atlantic Meridional Overturning Circulation (Beal et al., 2011; Biastoch et al., 2008; Marsh et al., 2007). The ability of such mesoscale eddies to be efficient in tracer transport, as well as the geographical characteristics of the heat, salt, or biogeochemical properties redistribution they induce, is directly controlled by their longevity and energy decay properties.

Although the processes responsible for the formation of LCRs have been (and remains) the focus of intense research (e.g. Candela et al. (2002); Oey et al. (2003); Lugo-Fernández et al. (2016); Donohue et al. (2016); Le Hénaff et al. (2023)), the processes responsible for their decay have received less attention. As of now, the decay of LCRs has been largely attributed to two processes : vortex-splitting (Forristall et al., 1992; Biggs et al., 1996; Lipphardt et al., 2008) and topographic interactions along the western GoM's continental slope, which was consequently nicknamed the *eddy graveyard* (Biggs, 1992; Vidal et al., 1994; Hamilton et al., 1999). However, these studies were all mostly descriptive and limited to a small number of eddies, and did not provide large-number statistics on the decay of LCRs based on a solid metric such as energy.

Using 25 years of satellite altimetry and a convenient empirical relationship between sea surface height (SSH) and heat content, T. Meunier et al. (2020) showed that, on average, LCRs have already lost over two thirds of their heat content before they reach the so-called *eddy graveyard*, and that heat decays at an inverse exponential rate right from the start of LCRs' life cycle, so that some other processes have to be invoked for the decay of LCR's heat content.

Beyond vortex-splitting and topographic effects, many processes can participate in the decay of a mesoscale eddy. These include Frontal instability (Brannigan et al., 2017; Pérez et al., 2022), Interaction with submesoscale eddies (de Marez et al., 2020; Jouanno et al., 2016; Tedesco et al., 2019), Mesoscale straining (Mariotti et al., 1994), Layering and double diffusion (Schmitt et al., 1986; Armi et al., 1989; Meunier et al., 2015; Middleton et al., 2021), interaction with internal gravity waves (Kunze, 1986; Polzin, 2008; Joyce et al., 2013), surface heat fluxes (Dewar, 1987), or wind-current interactions (Dewar & Flierl, 1987; Duhaut & Straub, 2006; Renault, Molemaker, Gula, et al., 2016).

Of all these processes, wind-current interactions in the form of current feedback on the wind stress are of special interest, since the latter was shown numerically to yield a reduction of 20 to 35 % of eddy kinetic energy in eddying currents (Duhaut & Straub, 2006; Renault, Molemaker, Gula, et al., 2016; Renault et al., 2017). This process, based on the simple idea that wind stress depends on relative wind speed in a frame of reference moving with the current, rather than absolute wind speed, has consequences in the wind-stress distribution over a mesoscale eddy. The wind stress is increased where the current opposes the wind, and decreased where the current flows in the direction of the wind. This results in a systematic negative wind stress work integrated over an eddy's surface, which extracts kinetic energy (KE) (Dewar & Flierl, 1987), as well as Ekman pumping which induces a negative buoyancy flux that converts available potential energy (APE) into KE (Gaube et al., 2015; Wilder et al., 2022). While these processes were studied in depth in eddying current systems using regional numerical models (Renault, Molemaker, Gula, et al., 2016; Renault et al., 2017), their impact on individual mesoscale eddies remains largely unknown apart from the extremely idealized studies of Dewar and Flierl (1987) and Wilder et al. (2022), which suggest a significant impact of current-feedback on numerical, isolated, idealized eddies. However, observational evidence of the impact of current-feedback on mesoscale eddies are still lacking.

Recently, T. Meunier et al. (2022) applied an empirical method known as the gravest empirical mode method (GEM) (Watts et al., 2001; Sun & Watts, 2001) to reconstruct the daily three-dimensional temperature and salinity structure of all LCRs detached in the GoM between 1993 and 2022. Their method was validated against *in situ* glider observations, and showed a striking accuracy (coefficient of determination R^2 greater than 0.93 between the GEM-reconstructed and the directly observed fields).

In this paper, we take advantage of this validated reconstruction method to estimate the energy decay properties, in time and space, of 40 LCRs detached between 1993 and 2023. Using scatterometer and reanalysis wind products, we also estimate the effect of current feedback on the decay and conversion of the eddies' energy. Beyond a regional study of some particular class of eddy, to the best of our knowledge, this work is the first systematic observation-based statistical study of the energy decay of mesoscale eddies, as well as the first observation-based estimate of the relative impact of wind-current interactions on the decay and conversion of eddies' energy. The results of this study could therefore provide some insight on the processes controlling mesoscale eddy decay in the ocean.

2 Data

This work is largely based on altimeter-derived sea surface height (SSH) observations. We use daily AVISO absolute dynamic topography (ADT) gridded fields. The grid has a $1/4^\circ$ degree resolution and the data is available from January 1st 1993 until now.

We also use nearly 7000 Argo profiles distributed over the entire deep GoM (Fig. 1a). Most of these floats were launched as part of the National Academies of Sciences Understanding Gulf Ocean Systems (UGOS) program.

The main wind product used is IFREMER CERSAT Global Blended Mean Wind Fields, which combines scatterometer observations with ECMWF operational wind analyses. The product is available on a $1/4^\circ$ grid every 6 hours. A 24 hours averaging was performed to coincide with the ADT observations. Detailed information as well as a retrospective study of the product's performance can be found in Desbiolles et al. (2017). Because Scatterometers estimate wind from the sea-state, and the latter depends on relative wind speed rather than absolute wind speed, their wind products are known to retain some signal of the current feedback (Plagge et al., 2012). Although this effect is attenuated by the gridding process, we compared the scatterometer product's results with data from ECMWF's ERA5 reanalysis, which provides estimates of the absolute wind. ERA5 is based on a 4DVAR ensemble data assimilating atmospheric model and is distributed as hourly outputs on a $1/4^\circ$ grid. Here, a 24 hours averaging was also performed. Full details about the methods can be found in Hersbach et al. (2020).

For both wind products, wind stress was computed using the COARE3.5 parameterization (Edson et al., 2013).

3 Methods

3.1 Theoretical background

In this study, we seek to describe the time evolution of the total mechanical energy of individual eddies, which is the three-dimensional integral of energy density over the eddy's volume.

The evolution equation for kinetic energy density ($E_k = \frac{1}{2}\rho|\mathbf{u}|^2$) reads (Gill, 1982):

$$\frac{DE_k}{Dt} + \rho'gw = -\nabla \cdot P'\mathbf{u} + \mathbf{u} \cdot \frac{\partial \boldsymbol{\tau}}{\partial z} + \nabla \cdot \mathbf{K}\nabla E_k + \rho\epsilon, \quad (1)$$

where E_k is kinetic energy, $\frac{D}{Dt}$ is the material derivative, ρ' is density anomaly referenced to a minimum potential energy profile, w is vertical velocity, P' is pressure anomaly, \mathbf{u} is the velocity vector, $\boldsymbol{\tau}$ is the wind stress, z is the vertical coordinate, \mathbf{K} is a diagonal diffusivity coefficient tensor and ϵ is the energy dissipation rate.

The second term on the left-hand side is the buoyancy flux, and is equal to the material rate of change of available potential energy density (Holliday & McIntyre, 1981):

$$\frac{DE_p}{Dt} = \rho'gw, \quad (2)$$

so that the left-hand side of equation (1) represents the material rate of change of total mechanical energy density ($E_m = E_k + E_p$). Still following Holliday and McIntyre (1981), available potential energy density is defined as:

$$E_p = -\int_0^\eta g\tilde{\eta} \frac{\partial \rho_r}{\partial z} (z - \tilde{\eta}) d\tilde{\eta}, \quad (3)$$

where ρ_r is the reference minimum potential energy profile and η is the isopycnal displacement, relative to the reference profile. In this work, we study the effects of the (relative) wind on energy decay and energy conversion, and we compute the buoyancy flux of equation (2) using the non-linear Ekman pumping vertical velocity (Stern, 1965) :

$$w_e = \frac{1}{\rho_0} \nabla \times \left(\frac{\boldsymbol{\tau}}{f + \zeta} \right) \quad (4)$$

Note that computing the non-forced vertical velocity using the Omega equation was also considered, but, since the estimated fields are not necessarily solutions of any equation

149 of motion, and given the relatively low spatial resolution, the omega-derived vertical ve-
 150 locity is essentially noise, with zero-mean vertical velocity.

151 As mentioned above, the wind stress to be considered here is the relative wind stress,
 152 which takes into account the feedback of the current and reads :

$$\boldsymbol{\tau} = \rho_a C_d |\mathbf{u}_a - \alpha \mathbf{u}_g| (\mathbf{u}_a - \alpha \mathbf{u}_g), \quad (5)$$

153 where ρ_a is air density, C_d is the drag coefficient computed using the COARE3.5 param-
 154 eterization (Edson et al., 2013), \mathbf{u}_a is the absolute wind velocity 10 m above the sea sur-
 155 face and \mathbf{u}_g is the velocity of the surface current, computed from the altimetry-derived
 156 SSH using the geostrophic balance assumption. α is a coefficient applied to the current
 157 velocity to account for the feedback of the stress increase/reduction by the current-feedback
 158 through frictional effects, that results in a reduction/increase of the absolute wind speed
 159 (Renault, Molemaker, McWilliams, et al., 2016). We used values of 1 and 0.7, following
 160 empirical results of Renault et al. (2019).

161 We are interested in quantifying the evolution of the total energy (\mathbb{E}_m) transported
 162 by an eddy whose boundary is defined by the closed line \mathcal{C} which encircles the surface
 163 \mathcal{S} :

$$\mathbb{E}_m = \iint_{\mathcal{S}} \int_{-H}^0 E_m dz ds, \quad (6)$$

164 where ds is a surface element and H is the eddy's thickness. We do not make the hy-
 165 pothesis that the boundary \mathcal{C} is a material line. Integrating the left hand side of equa-
 166 tion (1) in its flux form, using the Ostrogradski theorem, the Leibniz theorem, and the
 167 Reynolds transport theorem, we get an exact equation for the evolution of total mechan-
 168 ical energy, under the assumption that the thickness does not vary :

$$\begin{aligned} \frac{d}{dt} \mathbb{E}_m = \int_{-H}^0 \left\{ \underbrace{\oint_{\mathcal{C}} (\mathbf{u}_c - \mathbf{u}) \cdot \mathbf{n} E_m dl}_{(a)} - \underbrace{\oint_{\mathcal{C}} \mathbf{u} \cdot \mathbf{n} P' dl}_{(b)} + \underbrace{\iint_{\mathcal{S}} \mathbf{u} \cdot \frac{\partial \boldsymbol{\tau}}{\partial z} ds}_{(c)} \right. \\ \left. + \underbrace{\oint_{\mathcal{C}} \mathbf{K} \nabla E_k \cdot \mathbf{n} dl}_{(d)} + \underbrace{\iint_{\mathcal{S}} \rho \epsilon ds}_{(e)} \right\} dz \quad (7) \end{aligned}$$

169 The first term on the right hand side represents the energy flux through the eddy's
 170 boundary that is caused by the relative flow in the eddy's moving referential. In the case
 171 of a Lagrangian coherent vortex, the boundary \mathcal{C} is a material line, so that it is exactly
 172 advected by the flow ($\mathbf{u}_c = \mathbf{u}$) and the term vanishes. the second term is the work of
 173 the pressure force. Under the geostrophic approximation, it is null whatever the bound-
 174 ary. The third term is the wind stress work. Since the wind stress is dependent on the
 175 relative wind speed, even an homogeneous wind will exert some work, whose integral over
 176 the eddy's surface will be negative, whatever the vorticity sign (Dewar & Flierl, 1987).
 177 The viscous terms (d) represent all the unresolved (sub-grid scale) advective turbulent
 178 processes that might cause an energy flux through the eddy's boundary (which is only
 179 defined using coarse resolution observations) and the dissipation term (e) is essentially
 180 related to small scale turbulence yielding conversion of mechanical energy to internal en-
 181 ergy.

182 Because we are interested in examining and comparing the energy evolution of a
 183 set of eddies of different sizes, we need to use a normalized metric. The surface-averaged
 184 energy is a convenient variable:

$$\bar{E}_m = \frac{\mathbb{E}_m}{S}. \quad (8)$$

185 Integrating equation (7) with respect to time and dividing by the instantaneous
186 area of the eddy, we get an equation for the surface-averaged energy density.

$$\bar{E}_m(t) = \frac{1}{S} \int_0^t \int_{-H}^0 \{(a) + (b) + (c) + (d) + (e)\} dz d\tau \quad (9)$$

187 Since our purpose is to compute statistical properties of energy decay by ensemble-
188 averaging over all the detached eddies, using the surface-averaged energy density is con-
189 venient. Ensemble averaging using the integrated total energy would introduce a bias
190 by increasing the weight of large eddies in the average. Normalizing total energy by each
191 eddy's area avoids this bias. More interestingly, normalizing energy by the eddy's area
192 also removes the effects of energy loss due to direct loss or gain of area (hence mass), as
193 can happen during filamentation or splitting/merging events. For the sake of concision,
194 in the rest of the paper, the terms KE, APE and TE will be used to designate the sur-
195 face averaged kinetic, potential and total mechanical energy density. When studying the
196 impact of the current-modified wind stress on the eddies' energy, the two variables we
197 will focus on are the surface-averaged, time-integrated wind stress work, normalized by
198 the TE's initial value of each eddy that we will casually refer to as the wind stress work
199 (WSW), and the surface-averaged, time-integrated Ekman buoyancy flux, normalized
200 by the initial value of APE of each eddy, that we will casually refer to as the Ekman buoy-
201 ancy flux (EBF) :

$$\text{WSW}(t) = \frac{1}{\bar{E}_m(0)} \frac{\int_0^t \iint_{\mathcal{S}} \boldsymbol{\tau}(\tilde{t}) \cdot \mathbf{u}_g(\tilde{t}) ds d\tilde{t}}{S(t)}, \quad (10)$$

$$\text{EBF}(t) = \frac{1}{\bar{E}_p(0)} \frac{\int_0^t \int_{-H}^0 \iint_{\mathcal{S}} \rho' g w_e ds dz d\tilde{t}}{S(t)}. \quad (11)$$

203 3.2 The gravest empirical mode method (GEM)

204 To estimate the daily 3D structure of temperature and salinity (hence geostrophic
205 velocity, KE and APE density) from satellite altimetry, we use an empirical method known
206 as the gravest empirical mode projection (GEM) (Watts et al., 2001; Sun & Watts, 2001;
207 T. Meunier et al., 2022). It consists of establishing an empirical relationship between the
208 vertical thermohaline structure of the ocean and the dynamic height to build transfer
209 functions that associate one single value of temperature and salinity for each couple {pressure,
210 SSH}. The procedure used here was used and validated in the Gulf of Mexico and is de-
211 scribed in details in T. Meunier et al. (2022). The mean yearly transfer functions for salin-
212 ity and temperature are shown in Figure 1c and d, respectively : the downward sloping
213 of the isotherms and of the subsurface salinity maximum with increasing SSH, associ-
214 ated with the subtropical underwater (SUW) carried by LCRs is evident. Note that, to
215 account for the seasonality of surface conditions, which affects the accuracy of the three-
216 dimensional reconstruction in the top 200 dbar, the GEM fields were constructed on a
217 monthly basis. An example of APE and KE density cross-section reconstructed using
218 the GEM along with an average LCR's SSH anomaly is shown in Figure 1e and f, respec-
219 tively. APE is concentrated in the core of the eddy, while KE is stronger near the edges,
220 where density gradients are sharper. The APE maximum is 2.5 times larger than the KE
221 maximum and, when integrated over the whole LCR, APE largely dominates over KE
222 (T. Meunier et al., 2022).

223

3.3 Eddies' edge definition

224

225

226

227

228

229

230

231

232

233

234

235

236

237

238

239

240

241

242

243

244

245

246

247

248

249

250

251

252

253

254

255

256

In this work, we aim to follow the whole LCR, and not only its coherent part, which is usually confined to a small portion of the core (Beron-Vera et al., 2018; Andrade-Canto et al., 2020). Hence, rather than tracking so called Lagrangian coherent vortices (Haller & Beron-Vera, 2013; Beron-Vera et al., 2013), the eddy as we wish to track it should be defined as a compact rotating body of water detached from the LC, regardless of its *a priori* conservation properties. The detection and tracking method is based on ADT. First we define the LC's edge as the smallest-value ADT contour linking the Yucatan channel and the Florida strait. This contour usually encloses closed ADT contours, which are the signature of unborn LCRs. We define LCR detachment as the instant at which none of the closed contours remain enclosed within the LC anymore. Once detached, to define the LCR's boundary, we use a mixed Eulerian-Lagrangian procedure : at $t=0$ (detachment date), we initialize a cluster of virtual Lagrangian particles within the outermost closed SSH contour, which coincides with the boundary of the water mass detached from the LC. These particles are distributed on a $1\text{ km}\times 1\text{ km}$ regular grid. They are then integrated in the geostrophic surface velocity field inferred from the altimetry product, using a fourth-order Runge-Kutta scheme (Butcher, 1996). The particle concentration is then computed and interpolated on a regular $1/48^\circ$ grid. The LCR's edge is defined as the concentration contour with the original value at $t=0$, that is, the closed isopleth that encloses a compact surface of constant concentration equal to the original concentration. A sequence of particle concentration maps during the drift of LCR Poseidon in April and November 2016 is shown on figure 1g and h. The edge contour based on the concentration criterion is compared to two other Eulerian criteria : the Maximum velocity contour and the last closed SSH contour. While particle loss through filamentation of the eddy is evident, concentration within the eddy's boundary remain largely homogeneous. It is important to note that, while the method is based on Lagrangian particles integration, it does not belong to the class of *Lagrangian methods*, that seek coherent eddy boundaries, such as the null geodesics rings of Haller and Beron-Vera (2013) and Beron-Vera et al. (2018). Here, the boundary does not ensure the coherence of the eddy, in the sense that tracer conservation is not guaranteed (and our detected eddies actually do loose tracer). However, contrary to Lagrangian Coherent Vortices detected using proper *Lagrangian methods*, this method allows us to follow the entire body of water detached from the LC, and not only a small fragment of it. The initial boundaries of all eddies are shown in Figure 1b, where the SSH at the eddies' centers is color-coded.

257

4 Results

258

259

260

261

262

263

264

265

266

267

268

269

270

271

272

273

274

Individual trajectories of the 40 LCRs are shown on Figure 2a. TE, normalized by the initial values at the time of detachment, is color-coded. While a few LCRs maintain high levels of energy ($>80\%$) past the Campeche bank, west of 93°W , the vast majority start losing energy soon in their life cycle in the eastern GoM. The ensemble average of normalized TE for all LCRs is shown in Figures 2b. The circles' size represents the average diameter of LCRs during their drift. After 200 days, the average TE left in the eddies is only 26 % of the initial value at detachment. This value is of 21 and 28 % for KE and APE, respectively (not shown).

The evolution of the mean KE, APE and TE (non-normalized by initial values) is shown against time and longitude on figure 2c. The 95% confidence interval, computed using the bootstrap method, is shown as the light shaded areas. APE largely dominates over KE during the entire eddies' life cycle. On average, both KE and APE start decaying right from the first days after detachment and keep on decaying continuously with time until 200 days, resulting in a similar decay of TE. The average halving time for KE, APE and TE is of 101 days, 120 days, and 117 days, respectively. Looking at the longitude-dependence of energy, a similar pattern appears : APE and KE start decaying in the eastern basin near 88.5°W and decay continuously across the entire GoM. The halving lon-

275 gitude is of 91°W for KE and 91.6°W for APE and TE. The energy decay rates (Fig-
 276 ure 2d) not only confirm that energy loss occurs all along the eddies' drift through the
 277 GoM, but also that LCRs lose APE (and TE) at a faster rate in the eastern GoM, dur-
 278 ing the first month of their life cycle. KE does not exhibit this increased decay rate in
 279 the eastern basin, and decays regularly all along the eddies life cycle.

280 Since previous works have pointed out some critical longitude ($\approx 92\text{-}93^\circ\text{W}$) where
 281 eddies seem to decay at a faster rate, mostly because of instability and eddy-splitting
 282 (direct loss of mass; see Lipphardt et al. (2008) and references therein), we also inves-
 283 tigated the evolution of the total LCRs energy (the energy density integrated over the
 284 full eddy's surface and not the energy per unit area discussed above) as well as the evo-
 285 lution of the eddies area, which would clearly indicate regions of more frequent splitting.
 286 The surface integrated KE, APE and TE, normalized by their initial values and ensemble-
 287 averaged are shown against time and longitude in Figures 2e and f, respectively. As for
 288 the surface-averaged KE, TE and APE, the surface integrated KE, TE and APE smoothly
 289 and regularly decay with time during the whole LCRs life cycle. Similarly, the decay against
 290 longitude shows no obvious discontinuity, except for a slightly faster decay between 90
 291 and 91°W . The evolution of the ensemble-averaged LCRs areas against time and lon-
 292 gitude shows the same regular decay, without any evident discontinuity.

293 Equation (7) shows that for a mesoscale geostrophic eddy, where the work of the
 294 pressure force is negligible, TE can only decay through the action of wind stress work,
 295 an energy flux through the boundary, and diffusivity. As mentioned above, the energy
 296 flux through the boundary is impossible to estimate, since the boundary's velocity is un-
 297 definable (because it is not defined by a series of material points, or material line), and
 298 the diffusive term can not be estimated with satellite altimetry and Argo data only. On
 299 the other hand, the effects of wind stress work can be assessed using wind observations.
 300 Similarly, the decay of APE is directly linked to buoyancy fluxes (Equation 3), and while
 301 the vertical velocity can not be fully estimated, we still can estimate the contribution
 302 of Ekman pumping to it (Equation 4). In other words, while this work does not allow
 303 for a full budget of the energy equation, the effects of relative wind stress can be assessed
 304 effectively. Figure 2g compares the average evolution of TE (normalized by initial val-
 305 ues) to the effects of wind stress work for 4 different wind stress parametrization : ab-
 306 solute wind stress obtained from scatterometer products (SCAT abs), relative wind stress
 307 obtained from scatterometer products and computed by removing the full current ve-
 308 locity from the absolute wind value (SCAT rel), relative wind stress obtained from the
 309 ERA5 reanalysis and computed by removing the full current velocity from the absolute
 310 wind value (ERA rel), and relative wind stress obtained from scatterometer products and
 311 computed by removing 70 % of the current velocity to the absolute wind value (SCAT
 312 rel07). Relative wind stress work appears to contribute to the decay of the LCRs' TE,
 313 with an average of 18% and 15% of the original TE extracted when using Scatterome-
 314 ter and ERA5 wind products, respectively. This corresponds to respectively a quarter
 315 and a fifth of the energy lost by LCRs in 200 days. When using Renault et al. (2019)'s
 316 parameterization which uses a current velocity reduced by 30% to compute relative wind
 317 stress (SCAT rel07), we find that, on average, wind stress work then only accounts for
 318 about 10 % of the TE loss in LCRs. In all three cases, energy decay through wind stress
 319 work is faster in the beginning of the LCR's life cycle, and after about 120 days, wind
 320 stress work does not extract energy any more. For comparison, the work of the absolute
 321 wind was also computed. Surprisingly, it represents an energy source for LCRs with an
 322 average increase of the original TE by about 20% after 200 days. This shows that the
 323 mean spatial distribution of absolute wind in the GoM tends to increase LCRs energy,
 324 showing that the energy sink is really related to wind-current interactions.

325 Time evolution of APE is compared to the effects of Ekman buoyancy fluxes in fig-
 326 ure 2h. The wind parameterizations shown are the same as for Figure 2g. The close co-
 327 incidence of the decay of APE and that expected from Ekman buoyancy fluxes computed
 328 from scatterometer-derived relative wind stress is striking. It suggests that Ekman buoy-
 329 ancy fluxes might account for the whole observed APE decay. Using ERA5 relative wind

330 stress, we find that Ekman buoyancy flux accounts for a slightly reduced part of the APE
 331 decay (70 % of the APE loss after 200 days), and using the reduced current parameter-
 332 ization for relative wind stress computation (SCAT abs07), Ekman buoyancy flux ac-
 333 counts for about 65% of the total APE loss in 200 days. Using absolute wind stress, we
 334 find that Ekman buoyancy flux corresponds to an APE increase of nearly 20% during
 335 the first 170 days, followed by a small decrease in the last 30 days.

336 5 Discussion and conclusion

337 Using an observation-based method, we assessed the statistical properties of the
 338 energy decay of all LCRs detached since 1993. To the best of our knowledge, this is the
 339 first time such statistics on the energy decay of mesoscale eddies are obtained anywhere
 340 in the World ocean based on an observations.

341 We showed that LCRs' energy decay is a fast process occurring continuously dur-
 342 ing the whole eddies' life cycles. This observation is in contradiction with the commonly
 343 accepted idea that LCRs steadily drift through the GoM, retaining their hydrographic
 344 properties until they collapse against the western platform, as explicitly shown in the
 345 numerical simulations of Romanou et al. (2004), and suggested in a number of other nu-
 346 merical studies listed in Lipphardt et al. (2008) (Sturges et al., 1993; Dietrich et al., 1997;
 347 Kantha et al., 2005). However, it should be pointed out that our results do not contra-
 348 dict the idea of an *eddy graveyard*, but clearly show that the decay of LCRs does not hap-
 349 pen only there, but starts right from the first month after detachment from the LC and
 350 continues all along their life cycle. As they reach the so-called graveyard, LCRs are al-
 351 ready old and weak eddies that have typically lost over 3/4 of their energy. Topographic
 352 effects in the western basin can therefore not be considered a major cause of LCRs de-
 353 cay, but rather the ultimate process dispersing their remnants. Moreover, the energy de-
 354 cay rate was shown to be faster in the eastern basin soon after detachment than in the
 355 western basin, and the halving longitude is found as far East as 91.5°W.

356 Our results also contradict another long-standing claim that there exists some crit-
 357 ical longitude in the GoM, between 92 and 93°W, beyond which LCRs suddenly decay
 358 at a fast rate, mostly through low wavenumber instability (the observed elliptization of
 359 the eddies seems consistent with the development of an azimuthal mode 2 vortex Rossby
 360 wave) yielding vortex-splitting (Hamilton et al., 1999; Vukovich, 2007; Lipphardt et al.,
 361 2008). Although we acknowledge that LCRs might become unstable, loose coherence or
 362 split as directly observed by Biggs et al. (1996), so that increased decay rate might oc-
 363 casionally occur in the central basin, our results show no sign of a critical longitude be-
 364 tween 92 and 93 °W (nor anywhere) where LCRs loose mass or energy at a faster rate,
 365 and the decay of the eddies' area and surface-integrated KE, APE and TE is a gradual
 366 process occurring all through their life cycles.

367 Beyond the description of the decay of energy in LCRs, we also investigated the
 368 possible role of wind-current feedback on that decay. We showed that the effect of rel-
 369 ative wind stress work is non-negligible, but likely not a leading order mechanism in the
 370 decay of kinetic energy (and total mechanical energy) as it accounts for 25 and 20 % of
 371 the total energy loss in 200 days when using scatterometer and ERA5 wind fields, re-
 372 spectively. When using Renault et al. (2019)'s parameterization to account for the dimin-
 373 ution of absolute wind when the current opposes the wind (and *vice versa*) (by reducing
 374 the current velocity by 30 % when computing relative wind stress), we found that wind
 375 stress work then only accounts for 10 % of the total energy loss in 200 days.

376 However, the impact of current-feedback was shown to be important for the decay
 377 of APE, which would be entirely driven by Ekman buoyancy flux when using relative
 378 wind stress computed from scatterometer data. Beyond this striking result, the control
 379 of APE loss by Ekman buoyancy flux has implications on the decay of KE. Buoyancy
 380 flux does not extract TE: it converts APE to KE (it is often referred to as the baroclinic
 381 conversion term), which means that all along the LCRs life cycle, KE is fueled by this
 382 conversion. Given the modest role of wind stress work, this means that some other pro-

cesses, such as turbulent diffusivity at the edges of the eddies (subgrid-scale advective processes that are unresolved by the altimetry grid) might be important in the decay of LCRs' TE through the decay of KE.

Of course, our study does not allow estimation of the impact of direct energy flux through the eddies' boundary which is related to the fact that the edges we consider are not material lines (term (a) in equation 7). This is clearly a caveat of not using Lagrangian coherent boundaries, which would ensure the flux term to be zero, and would allow us to estimate the diffusive term as it would become the only unknown of Equation (7). The choice not to use such Lagrangian metrics was motivated by the need to estimate the evolution of the full detached patch of LC water, and not only a small piece of its core. In particular, relative wind stress work becomes important near the edge of the eddies, where the velocity is maximum, while long-horizon coherent LCRs usually exclude this peripheral part. However, working with three-dimensional Lagrangian objective eddy framing (Beron-Vera et al., 2013; Haller & Beron-Vera, 2013) would be complementary to this study. Although it would only allow to estimate the properties and fate of the inner core of LCRs, it could allow to study more accurately the impact of Ekman buoyancy fluxes in baroclinic conversion. Such study is currently in progress.

Note that, while this study is focused on the GoM, similar processes are expected to occur in other warm-core rings (e.g. Agulhas rings, Gulf stream rings, Mozambic channel rings, North Brazil Current rings, Kuroshio rings etc.) and a similar study, dedicated to the decay of Agulhas rings is also in progress.

6 Open Research

All data used in this study are publicly available. The gridded scatterometer wind product and the absolute dynamic topography SSH product are available from Copernicus (<https://data.marine.copernicus.eu>). Direct link to the wind product dataset is also available at <https://www.pigma.org/geonetwork/srv/api/records/85c907d3-98fc-4ce7-b7e4-7332aa3fe660>. Direct link to the ADT product is also available at https://data.marine.copernicus.eu/product/SEALEVEL_GLO_PHY_CLIMATE_L4_MY_008_057/download. Data is available after users create a Copernicus account. Argo data are available from any data assembly center (e.g. <https://dataselection.euro-argo.eu/>), specifying the geographical limits of $[-99 -80]^{\circ}W$ and $[17 31]^{\circ}N$.

Acknowledgments

The authors are grateful to Amala Mahadevan, Mike Spall, Lionel Renault and Xavier Carton for their useful suggestions and comments. This work is part of the LC-floats and UGOS3 projects, funded by the US National Academy of Sciences through the Understanding Gulf Ocean Systems grants 2000010488 and 200013145.

References

- Andrade-Canto, F., Karrasch, D., & Beron-Vera, F. J. (2020, November). Genesis, evolution, and apocalypse of Loop Current rings. *Physics of Fluids*, *32*(11), 116603. doi: 10.1063/5.0030094
- Armi, L., Hebert, D., Oakey, N., Price, J. F., Richardson, P. L., Thomas Rossby, H., & Ruddick, B. (1989, March). Two Years in the Life of a Mediterranean Salt Lens. *Journal of Physical Oceanography*, *19*(3), 354-370. doi: 10.1175/1520-0485(1989)019<0354:TYITLO>2.0.CO;2
- Beal, L. r., De Ruijter, W. r. r., Biastoch, A., Zahn, R., & SCOR/WCRP/IAPSO Working Group 136. (2011, April). On the role of the Agulhas system in ocean circulation and climate. , *472*(7344), 429-436. doi: 10.1038/nature09983
- Beron-Vera, F. J., Olascoaga, M. J., Wang, Y., Triñanes, J., & Pérez-Brunius, P. (2018, July). Enduring Lagrangian coherence of a Loop Current ring as-

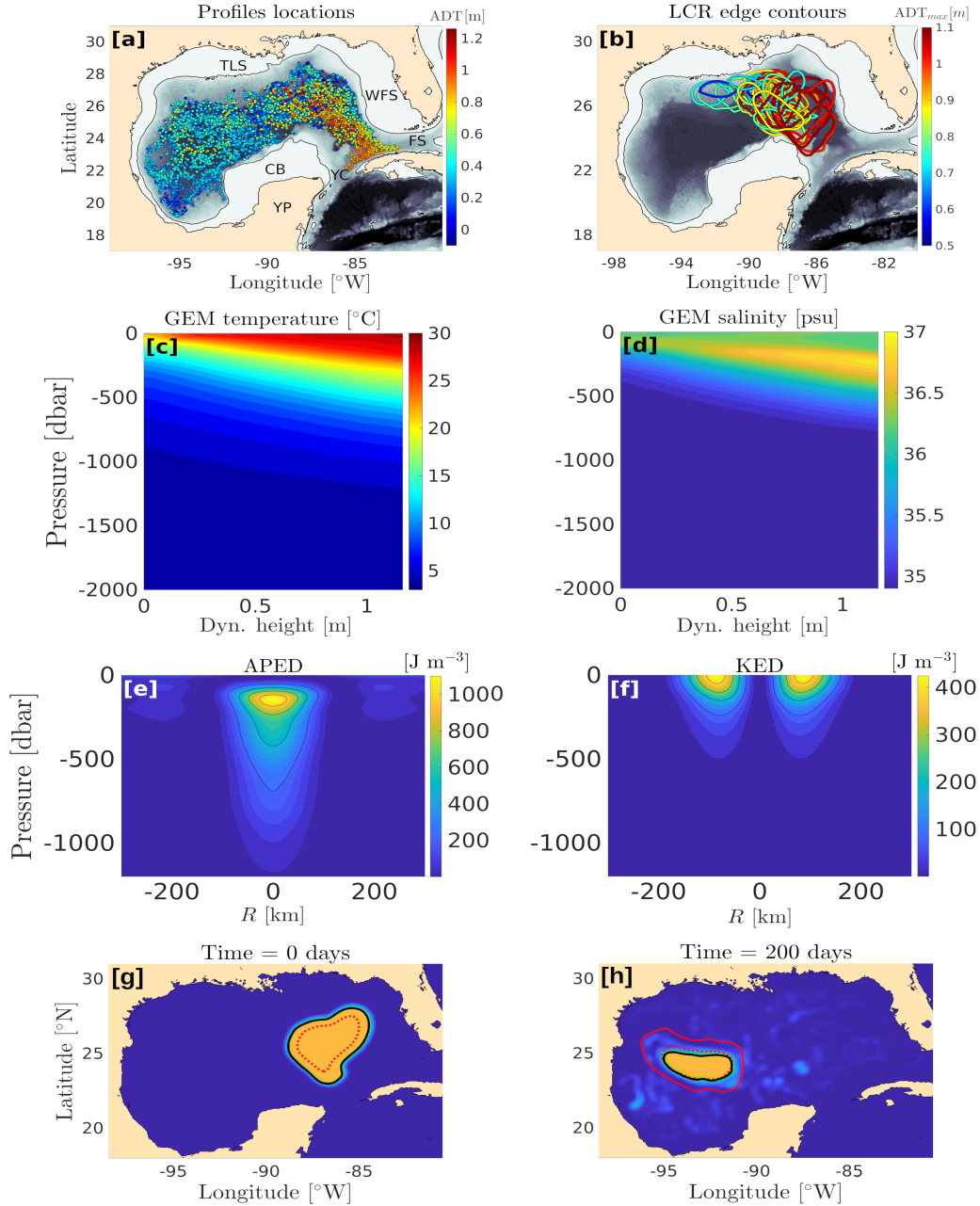


Figure 1. a: Location of the ARGO profiles used to build the Gravest Empirical Modes (GEM) for the Gulf of Mexico (GoM). The color code represents the local Absolute Dynamic Topography (ADT). The names of the GoM’s main topographic features are indicated. YC stands for Yucatan channel, FS stands for Florida strait, WFS stands for West Florida shelf, CB stands for Campeche bank, YP stands for Yucatan peninsula, and TLS stands for Texas-Louisiana shelf. b: Edge contours on the first day after detachment for all the Loop Current Rings (LCR) detached between 1993 and 2023. The color code represents ADT at the center of the eddy. c: GEM transfer function for temperature. The x-axis is dynamic height, the y-axis is pressure, and the color map is temperature. d: Same as (c) for salinity. e: Available potential energy density section across an average LCR reconstructed using the GEM method. f: same as (e) for kinetic energy density. g: Initial particle concentration in Loop Current Ring Poseidon on detachment date. The plain and dashed red lines represent the last closed ADT contour and the maximum velocity contour, respectively. Normalized passive tracer concentration is color-coded (yellow is 1 and dark blue is zero). The concentration-based edge contour of Poseidon is materialized as a thick black line. h: Same as (g) after 200 days—11—

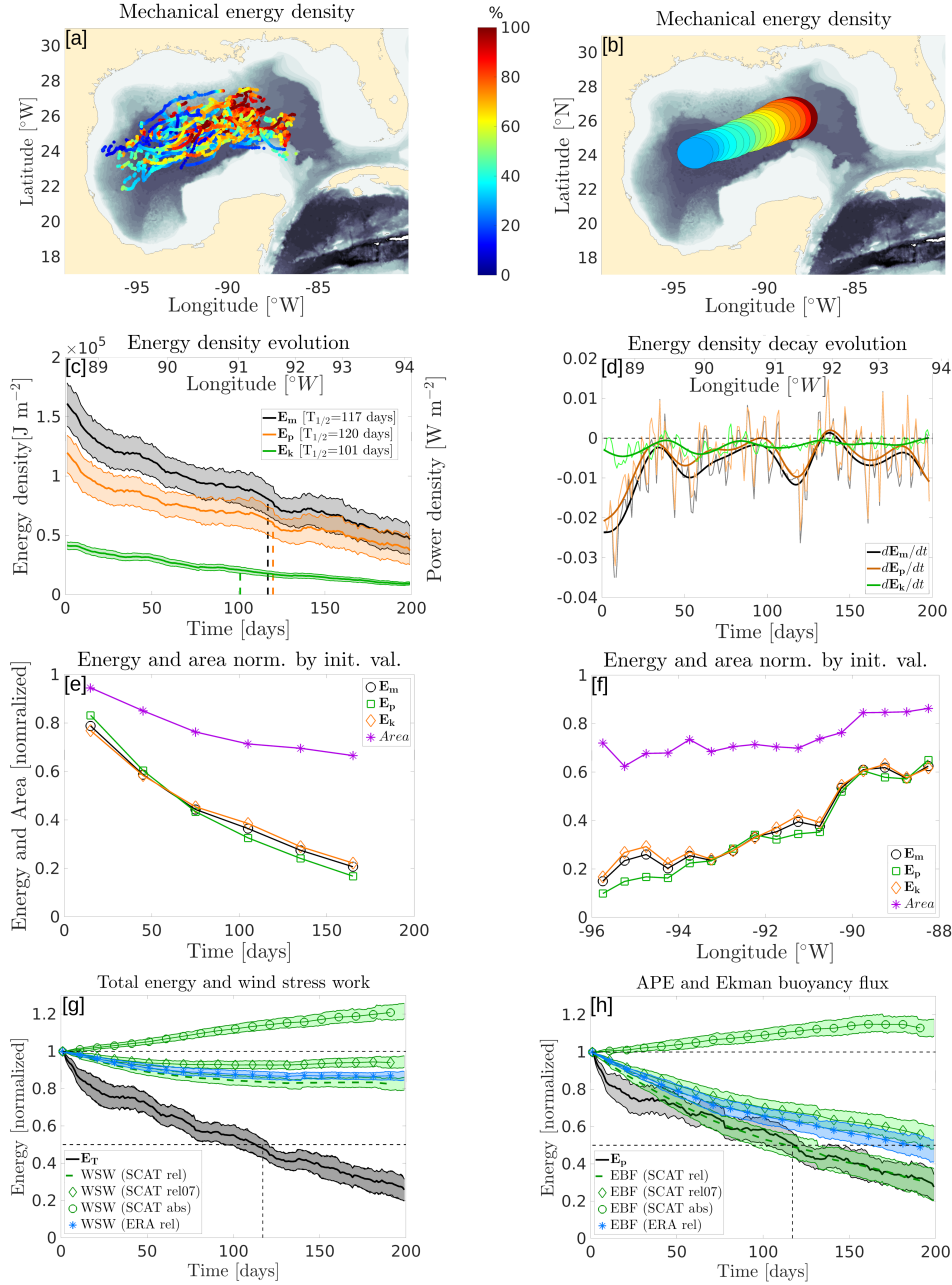


Figure 2. a: Trajectories of the center of the 40 Loop Current Rings (LCR). Total mechanical energy (TE) normalized by its initial value is color-coded. b: Ensemble-averaged TE normalized by its initial value. The position and diameter of the circles represent the average position and size of the LCRs. c: Time evolution of the average energy density. The black, orange and green lines represent total mechanical energy (TE), available potential energy (APE), and kinetic energy (KE), respectively. The light shaded areas around the lines represent the 95% confidence interval. The vertical dashed lines represent the energy halving time. The average longitude corresponding to the time is indicated on the top x-axis. d: Time evolution of the ensemble averaged rate of change of energy density (time derivative of energy density). The smooth dark thick lines represent the 30-days low pass filtered values, while the thin light lines represent the raw results. The color code is the same as in panel (c). e: Ensemble average of the non-surface-averaged KE (orange diamonds), TE (black circles) and APE (green squares) and eddy's area (purple stars) normalized by their initial values against time. f: Same as (e) against longitude. g: Energy extraction by the effects of wind stress work. The dashed line represents wind stress work computed from the scatterometer data. The green diamonds represent wind stress work computed by reducing the current by a factor of a 0.7 when computing relative wind. The red circles represent the effect of wind stress work computed using the absolute wind stress. The blue stars represent the effect of wind stress work computed using the ERA5 reanalysis. Time evolution of the TE is indicated as a black line. h: Energy conversion by the effect of the Ekman buoyancy flux. The Color code is the same as in panel (g). Time evolution of APE is indicated as the black line.

- 432 sessed using independent observations. *Scientific Reports*, 8, 11275. doi:
433 10.1038/s41598-018-29582-5
- 434 Beron-Vera, F. J., Wang, Y., Olascoaga, M. J., Goni, G. J., & Haller, G. (2013,
435 July). Objective Detection of Oceanic Eddies and the Agulhas Leak-
436 age. *Journal of Physical Oceanography*, 43(7), 1426-1438. doi: 10.1175/
437 JPO-D-12-0171.1
- 438 Biaostoch, A., Böning, C. W., & Lutjeharms, J. R. E. (2008, November). Agulhas
439 leakage dynamics affects decadal variability in Atlantic overturning circulation.
440 , 456(7221), 489-492. doi: 10.1038/nature07426
- 441 Biggs, D. C. (1992, February). Nutrients, plankton, and productivity in a
442 warm-core ring in the western Gulf of Mexico. , 97(C2), 2143-2154. doi:
443 10.1029/90JC02020
- 444 Biggs, D. C., Fargion, G. S., Hamilton, P., & Leben, R. R. (1996, September).
445 Cleavage of a Gulf of Mexico Loop Current eddy by a deep water cyclone. ,
446 101(C9), 20629-20642. doi: 10.1029/96JC01078
- 447 Bramnigan, L., Marshall, D. P., Naveira Garabato, A. C., Nurser, A. J. G., & Kaiser,
448 J. (2017, December). Submesoscale Instabilities in Mesoscale Eddies. *Journal*
449 *of Physical Oceanography*, 47(12), 3061-3085. doi: 10.1175/JPO-D-16-0178.1
- 450 Butcher, J. C. (1996). A history of runge-kutta methods. *Applied numerical mathe-*
451 *matics*, 20(3), 247-260.
- 452 Candela, J., Sheinbaum, J., Ochoa, J., Badan, A., & Leben, R. (2002, November).
453 The potential vorticity flux through the Yucatan Channel and the Loop Cur-
454 rent in the Gulf of Mexico. , 29(22), 2059. doi: 10.1029/2002GL015587
- 455 de Marez, C., Meunier, T., Morvan, M., L'Hégaret, P., & Carton, X. (2020, Febru-
456 ary). Study of the stability of a large realistic cyclonic eddy. *Ocean Modelling*,
457 146, 101540. doi: 10.1016/j.ocemod.2019.101540
- 458 Desbiolles, F., Bentamy, A., Blanke, B., Roy, C., Mestas-Nuñez, A. M., Grodsky,
459 S. A., ... Maes, C. (2017, April). Two decades [1992-2012] of surface wind
460 analyses based on satellite scatterometer observations. *Journal of Marine*
461 *Systems*, 168, 38-56. doi: 10.1016/j.jmarsys.2017.01.003
- 462 Dewar, W. K. (1987, December). Ventilating Warm Rings: Theory and Energet-
463 ics. *Journal of Physical Oceanography*, 17(12), 2219-2231. doi: 10.1175/1520
464 -0485(1987)017<2219:VWRTAE>2.0.CO;2
- 465 Dewar, W. K., & Flierl, G. R. (1987, October). Some Effects of the Wind
466 on Rings. *Journal of Physical Oceanography*, 17(10), 1653-1667. doi:
467 10.1175/1520-0485(1987)017<1653:SEOTWO>2.0.CO;2
- 468 Dietrich, D. E., Lin, C. A., Mestas-Nunez, A., & Ko, D. S. (1997, January). A
469 high resolution numerical study of Gulf of Mexico fronts and eddies. *Meteorol-*
470 *ogy and Atmospheric Physics*, 64(3-4), 187-201. doi: 10.1007/BF01029692
- 471 Donohue, K. A., Watts, D. R., Hamilton, P., Leben, R., & Kennelly, M. (2016, De-
472 cember). Loop Current Eddy formation and baroclinic instability. *Dynamics of*
473 *Atmospheres and Oceans*, 76, 195-216. doi: 10.1016/j.dynatmoce.2016.01.004
- 474 Duhaut, T. H. A., & Straub, D. N. (2006, January). Wind Stress Dependence
475 on Ocean Surface Velocity: Implications for Mechanical Energy Input to
476 Ocean Circulation. *Journal of Physical Oceanography*, 36(2), 202. doi:
477 10.1175/JPO2842.1
- 478 Edson, J. B., Jampana, V., Weller, R. A., Bigorre, S. P., Plueddemann, A. J.,
479 Fairall, C. W., ... Hersbach, H. (2013, August). On the Exchange of Mo-
480 mentum over the Open Ocean. *Journal of Physical Oceanography*, 43(8),
481 1589-1610. doi: 10.1175/JPO-D-12-0173.1
- 482 Elliott, B. A. (1982, November). Anticyclonic Rings in the Gulf of Mex-
483 ico. *Journal of Physical Oceanography*, 12(11), 1292-1309. doi: 10.1175/
484 1520-0485(1982)012<1292:ARITGO>2.0.CO;2
- 485 Forristall, G. Z., Schaudt, K. J., & Cooper, C. K. (1992, February). Evolution and
486 kinematics of a loop current eddy in the Gulf of Mexico during 1985. , 97(C2),

- 487 2173-2184. doi: 10.1029/91JC02905
- 488 Gaube, P., Chelton, D. B., Samelson, R. M., Schlax, M. G., & O'Neill, L. W.
489 (2015, January). Satellite Observations of Mesoscale Eddy-Induced Ek-
490 man Pumping. *Journal of Physical Oceanography*, *45*(1), 104-132. doi:
491 10.1175/JPO-D-14-0032.1
- 492 Haller, G., & Beron-Vera, F. J. (2013, September). Coherent Lagrangian vortices:
493 the black holes of turbulence. *Journal of Fluid Mechanics*, *731*, R4. doi: 10
494 .1017/jfm.2013.391
- 495 Hamilton, P., Fargion, G. S., & Biggs, D. C. (1999, June). Loop Current Eddy Paths
496 in the Western Gulf of Mexico. *Journal of Physical Oceanography*, *29*(6), 1180-
497 1207. doi: 10.1175/1520-0485(1999)029<1180:LCEPIT>2.0.CO;2
- 498 Hamilton, P., Leben, R., Bower, A., Furey, H., & Pérez-Brunius, P. (2018, April).
499 Hydrography of the Gulf of Mexico Using Autonomous Floats. *Journal of*
500 *Physical Oceanography*, *48*(4), 773-794. doi: 10.1175/JPO-D-17-0205.1
- 501 Hersbach, H., Bell, B., Berrisford, P., Hirahara, S., Horányi, A., Muñoz-Sabater,
502 J., ... Thépaut, J.-N. (2020, July). The ERA5 global reanalysis. *Quar-*
503 *terly Journal of the Royal Meteorological Society*, *146*(730), 1999-2049. doi:
504 10.1002/qj.3803
- 505 Holliday, D., & McIntyre, M. E. (1981, June). On potential energy density in an in-
506 compressible, stratified fluid. *Journal of Fluid Mechanics*, *107*, 221-225. doi:
507 10.1017/S0022112081001742
- 508 Jaimes, B., Shay, L. K., & Brewster, J. K. (2016, December). Observed air-
509 sea interactions in tropical cyclone Isaac over Loop Current mesoscale
510 eddy features. *Dynamics of Atmospheres and Oceans*, *76*, 306-324. doi:
511 10.1016/j.dynatmoce.2016.03.001
- 512 Jouanno, J., Ochoa, J., Pallàs-Sanz, E., Sheinbaum, J., Andrade-Canto, F., Can-
513 dela, J., & Molines, J.-M. (2016, November). Loop Current Frontal
514 Eddies: Formation along the Campeche Bank and Impact of Coastally
515 Trapped Waves. *Journal of Physical Oceanography*, *46*(11), 3339-3363. doi:
516 10.1175/JPO-D-16-0052.1
- 517 Joyce, T. M., Toole, J. M., Klein, P., & Thomas, L. N. (2013, April). A near-inertial
518 mode observed within a Gulf Stream warm-core ring. *Journal of Geophysical*
519 *Research (Oceans)*, *118*(4), 1797-1806. doi: 10.1002/jgrc.20141
- 520 Kantha, L., Choi, J.-K., Schaudt, K. J., & Cooper, C. K. (2005, January). A
521 regional data-assimilative model for operational use in the Gulf of Mexico.
522 *Washington DC American Geophysical Union Geophysical Monograph Series*,
523 *161*, 165-180. doi: 10.1029/161GM14
- 524 Kunze, E. (1986, August). The Mean and Near-Inertial Velocity Fields in a Warm-
525 Core Ring. *Journal of Physical Oceanography*, *16*(8), 1444-1461. doi: 10.1175/
526 1520-0485(1986)016<1444:TMANIV>2.0.CO;2
- 527 Leben, R. R. (2005, January). Altimeter-derived loop current metrics. *Washington*
528 *DC American Geophysical Union Geophysical Monograph Series*, *161*, 181-201.
529 doi: 10.1029/161GM15
- 530 Le Hénaff, M., Kourafalou, V. H., Androulidakis, Y., Ntaganou, N., & Kang, H.
531 (2023). Influence of the caribbean sea eddy field on loop current predictions.
532 *Frontiers in Marine Science*, *10*, 1129402.
- 533 Lipphardt, B. L., Poje, A. C., Kirwan, A. D., Kantha, L., & Zweng, M. (2008).
534 Death of three loop current rings. *Journal of Marine Research*, *66*(1), 25-60.
- 535 Lugo-Fernández, A., Leben, R. R., & Hall, C. A. (2016, December). Kine-
536 matic metrics of the Loop Current in the Gulf of Mexico from satellite
537 altimetry. *Dynamics of Atmospheres and Oceans*, *76*, 268-282. doi:
538 10.1016/j.dynatmoce.2016.01.002
- 539 Mariotti, A., Legras, B., & Dritschel, D. G. (1994, December). Vortex stripping and
540 the erosion of coherent structures in two-dimensional flows. *Physics of Fluids*,
541 *6*(12), 3954-3962. doi: 10.1063/1.868385

- 542 Marsh, R., Hazeleger, W., Yool, A., & Rohling, E. J. (2007, February). Stability of
543 the thermohaline circulation under millennial CO₂ forcing and two alternative
544 controls on Atlantic salinity. , *34*(3), L03605. doi: 10.1029/2006GL027815
- 545 Meunier, Ménesguen, C., Schopp, R., & Le Gentil, S. (2015). Tracer stirring around
546 a meddy: The formation of layering. *Journal of Physical Oceanography*, *45*(2),
547 407–423.
- 548 Meunier, T., Pérez-Brunius, P., & Bower, A. (2022, August). Reconstructing the
549 Three-Dimensional Structure of Loop Current Rings from Satellite Altime-
550 try and In Situ Data Using the Gravest Empirical Modes Method. *Remote*
551 *Sensing*, *14*(17), 4174. doi: 10.3390/rs14174174
- 552 Meunier, T., Sheinbaum, J., Pallàs-Sanz, E., Tenreiro, M., Ochoa, J., Ruiz-Angulo,
553 A., . . . de Marez, C. (2020, February). Heat Content Anomaly and Decay
554 of Warm-Core Rings: the Case of the Gulf of Mexico. , *47*(3), e85600. doi:
555 10.1029/2019GL085600
- 556 Middleton, L., Fine, E. C., MacKinnon, J. A., Alford, M. H., & Taylor, J. R. (2021,
557 August). Estimating Dissipation Rates Associated With Double Diffusion. ,
558 *48*(15), e92779. doi: 10.1029/2021GL092779
- 559 Molina, M. J., Timmer, R. P., & Allen, J. T. (2016, December). Importance of
560 the Gulf of Mexico as a climate driver for U.S. severe thunderstorm activity. ,
561 *43*(23), 12,295-12,304. doi: 10.1002/2016GL071603
- 562 Oey, L. Y., Lee, H. C., & Schmitz, W. J. (2003, October). Effects of winds and
563 Caribbean eddies on the frequency of Loop Current eddy shedding: A numer-
564 ical model study. *Journal of Geophysical Research (Oceans)*, *108*(C10), 3324.
565 doi: 10.1029/2002JC001698
- 566 Pérez, J. G. C., Pallàs-Sanz, E., Tenreiro, M., Meunier, T., Jouanno, J., & Ruiz-
567 Angulo, A. (2022, April). Overturning Instabilities Across a Warm Core Ring
568 From Glider Observations. *Journal of Geophysical Research (Oceans)*, *127*(4),
569 e2021JC017527. doi: 10.1029/2021JC017527
- 570 Plagge, A. M., Vandemark, D., & Chapron, B. (2012, December). Examining the
571 Impact of Surface Currents on Satellite Scatterometer and Altimeter Ocean
572 Winds. *Journal of Atmospheric and Oceanic Technology*, *29*(12), 1776-1793.
573 doi: 10.1175/JTECH-D-12-00017.1
- 574 Polzin, K. L. (2008, January). Mesoscale Eddy-Internal Wave Coupling. Part
575 I: Symmetry, Wave Capture, and Results from the Mid-Ocean Dynam-
576 ics Experiment. *Journal of Physical Oceanography*, *38*(11), 2556. doi:
577 10.1175/2008JPO3666.1
- 578 Renault, L., Marchesiello, P., Masson, S., & McWilliams, J. C. (2019, March).
579 Remarkable Control of Western Boundary Currents by Eddy Killing, a
580 Mechanical Air-Sea Coupling Process. , *46*(5), 2743-2751. doi: 10.1029/
581 2018GL081211
- 582 Renault, L., McWilliams, J. C., & Penven, P. (2017, August). Modulation of the Ag-
583 ulhas Current Retroreflection and Leakage by Oceanic Current Interaction with
584 the Atmosphere in Coupled Simulations. *Journal of Physical Oceanography*,
585 *47*(8), 2077-2100. doi: 10.1175/JPO-D-16-0168.1
- 586 Renault, L., Molemaker, M. J., Gula, J., Masson, S., & McWilliams, J. C. (2016,
587 November). Control and Stabilization of the Gulf Stream by Oceanic Current
588 Interaction with the Atmosphere. *Journal of Physical Oceanography*, *46*(11),
589 3439-3453. doi: 10.1175/JPO-D-16-0115.1
- 590 Renault, L., Molemaker, M. J., McWilliams, J. C., Shchepetkin, A. F., Lemarié, F.,
591 Chelton, D., . . . Hall, A. (2016, June). Modulation of Wind Work by Oceanic
592 Current Interaction with the Atmosphere. *Journal of Physical Oceanography*,
593 *46*(6), 1685-1704. doi: 10.1175/JPO-D-15-0232.1
- 594 Romanou, A., Chassignet, E. P., & Sturges, W. (2004, January). Gulf of Mexico
595 circulation within a high-resolution numerical simulation of the North Atlantic
596 Ocean. *Journal of Geophysical Research (Oceans)*, *109*(C1), C01003. doi:

- 597 10.1029/2003JC001770
 598 Schmitt, R. W., Lueck, R. G., & Joyce, T. M. (1986, November). Fine- and mi-
 599 crostructure at the edge of a warm-core ring. *Deep Sea Research A*, *33*(11-12),
 600 1665-1689. doi: 10.1016/0198-0149(86)90073-7
- 601 Shay, L. K., Goni, G. J., & Black, P. G. (2000). Effects of a warm oceanic feature on
 602 hurricane opal. *Mon. Weather Rev.*, *128*, 1366-1383.
- 603 Stern, M. E. (1965, January). Interaction of a uniform wind stress with a
 604 geostrophic vortex. *Deep Sea Research A*, *12*(3), 355-367. doi: 10.1016/
 605 0011-7471(65)90007-0
- 606 Sturges, W., Evans, J. C., Welsh, S., & Holland, W. (1993, February). Separation
 607 of Warm-Core Rings in the Gulf of Mexico. *Journal of Physical Oceanography*,
 608 *23*(2), 250-268. doi: 10.1175/1520-0485(1993)023<0250:SOWCRI>2.0.CO;2
- 609 Sun, C., & Watts, D. R. (2001, February). A circumpolar gravest empirical
 610 mode for the Southern Ocean hydrography. , *106*(C2), 2833-2855. doi:
 611 10.1029/2000JC900112
- 612 Tedesco, P., Gula, J., Ménesguen, C., Penven, P., & Krug, M. (2019, Novem-
 613 ber). Generation of Submesoscale Frontal Eddies in the Agulhas Cur-
 614 rent. *Journal of Geophysical Research (Oceans)*, *124*(11), 7606-7625. doi:
 615 10.1029/2019JC015229
- 616 Vidal, V. M. V., Vidal, F. V., Hernández, A. F., Meza, E., & Zambrano, L. (1994).
 617 Winter water mass distributions in the western gulf of mexico affected by a
 618 colliding anticyclonic ring. *Journal of Oceanography*, *50*, 559-588.
- 619 Vukovich, F. M. (2007, March). Climatology of Ocean Features in the Gulf of Mex-
 620 ico Using Satellite Remote Sensing Data. *Journal of Physical Oceanography*,
 621 *37*(3), 689-707. doi: 10.1175/JPO2989.1
- 622 Watts, D. R., Sun, C., & Rintoul, S. (2001, August). A Two-Dimensional Gravest
 623 Empirical Mode Determined from Hydrographic Observations in the Sub-
 624 antarctic Front. *Journal of Physical Oceanography*, *31*(8), 2186-2209. doi:
 625 10.1175/1520-0485(2001)031<2186:ATDGEM>2.0.CO;2
- 626 Wilder, T., Zhai, X., Munday, D., & Joshi, M. (2022). The response of a baroclinic
 627 anticyclonic eddy to relative wind stress forcing. *Journal of Physical Oceanog-
 628 raphy*.

The Energy Decay of Warm-core Eddies in the Gulf of Mexico

Thomas Meunier¹, Amy Bower¹, Paula Pérez-Brunius², and Federico Graef²

¹Woods Hole Oceanographic Institution, 360 Woods Hole road, Woods Hole, MA02543, USA

²CICESE, Carretera Ensenada-Tijuana 3918, Ensenada BC 22860, Mexico

Key Points:

- Time evolution of the energy of Warm-core rings in the Gulf of Mexico is assessed using empirical methods and satellite altimetry.
- The vast majority of mechanical energy (kinetic plus available potential) is lost early in the eddies life cycles, far from the western boundary.
- Wind-current feed back effects such as Ekman buoyancy flux and wind stress work play an important role in energy conversion and decay.

Abstract

The Gulf of Mexico (GoM) is home to some of the most energetic eddies in the ocean. They detach from the Loop-Current and drift through the basin, transporting large amounts of heat and salt. These eddies, known as Loop Current rings (LCRs) have a crucial role in the GoM's dynamics and in the weather of the eastern US, and this role is largely conditioned by their longevity and decay properties. Here, we use an empirical method to estimate the energy evolution of all LCRs detached since 1993. We found that, contrary to the commonly accepted idea that LCRs conserve their energy as they drift through the GoM and decay suddenly against the western platform, LCRs' energy decays faster in the eastern basin, and they typically lose three-quarter of their energy before encountering the continental shelf. We also show that wind-current feedback largely contributes to the energy decay and conversion.

Plain Language Summary

Ocean eddies can be long-lived and carry large amounts of heat and salt across ocean basins and marginal seas. This is the case of Loop Current rings (LCRs), which are large warm-core eddies drifting through the Gulf of Mexico (GoM). Understanding how these eddies lose their energy is key to understand their longevity and transport properties. Here, we use a previously validated empirical method based on *in situ* observations to estimate the time evolution of LCRs energy using satellite observations. We show that LCRs decay continuously during their life cycle, contrary to the previously accepted idea that they decay when collapsing against the western GoM's continental shelf. LCRs have already lost three-quarter of their energy before they reach any topographic obstacle. Using wind observations, we also show that wind-current interactions are key to the energy loss of these eddies.

1 Introduction

Coherent eddies can carry tracers across oceanic basins and participate in the transport of water-masses that impact large scale circulation and climate as well as ecosystems. For instance, Loop Current rings (LCRs), detaching from the Loop Current (LC), carry warm subtropical underwater (SUW) originating from the Caribbean through the Gulf of Mexico (Elliott, 1982; Leben, 2005) and have a direct impact on the basin's water mass properties (Vidal et al., 1994; Hamilton et al., 2018; T. Meunier et al., 2020), hurricane intensification (Shay et al., 2000; Jaimes et al., 2016), and thunderstorm occurrence east of the Rocky mountains (Molina et al., 2016). Similarly, Agulhas rings carry anomalously warm and salty Indian Ocean water through the South Atlantic and participate in the upper limb of the Atlantic Meridional Overturning Circulation (Beal et al., 2011; Biastoch et al., 2008; Marsh et al., 2007). The ability of such mesoscale eddies to be efficient in tracer transport, as well as the geographical characteristics of the heat, salt, or biogeochemical properties redistribution they induce, is directly controlled by their longevity and energy decay properties.

Although the processes responsible for the formation of LCRs have been (and remains) the focus of intense research (e.g. Candela et al. (2002); Oey et al. (2003); Lugo-Fernández et al. (2016); Donohue et al. (2016); Le Hénaff et al. (2023)), the processes responsible for their decay have received less attention. As of now, the decay of LCRs has been largely attributed to two processes : vortex-splitting (Forristall et al., 1992; Biggs et al., 1996; Lipphardt et al., 2008) and topographic interactions along the western GoM's continental slope, which was consequently nicknamed the *eddy graveyard* (Biggs, 1992; Vidal et al., 1994; Hamilton et al., 1999). However, these studies were all mostly descriptive and limited to a small number of eddies, and did not provide large-number statistics on the decay of LCRs based on a solid metric such as energy.

Using 25 years of satellite altimetry and a convenient empirical relationship between sea surface height (SSH) and heat content, T. Meunier et al. (2020) showed that, on average, LCRs have already lost over two thirds of their heat content before they reach the so-called *eddy graveyard*, and that heat decays at an inverse exponential rate right from the start of LCRs' life cycle, so that some other processes have to be invoked for the decay of LCR's heat content.

Beyond vortex-splitting and topographic effects, many processes can participate in the decay of a mesoscale eddy. These include Frontal instability (Brannigan et al., 2017; Pérez et al., 2022), Interaction with submesoscale eddies (de Marez et al., 2020; Jouanno et al., 2016; Tedesco et al., 2019), Mesoscale straining (Mariotti et al., 1994), Layering and double diffusion (Schmitt et al., 1986; Armi et al., 1989; Meunier et al., 2015; Middleton et al., 2021), interaction with internal gravity waves (Kunze, 1986; Polzin, 2008; Joyce et al., 2013), surface heat fluxes (Dewar, 1987), or wind-current interactions (Dewar & Flierl, 1987; Duhaut & Straub, 2006; Renault, Molemaker, Gula, et al., 2016).

Of all these processes, wind-current interactions in the form of current feedback on the wind stress are of special interest, since the latter was shown numerically to yield a reduction of 20 to 35 % of eddy kinetic energy in eddying currents (Duhaut & Straub, 2006; Renault, Molemaker, Gula, et al., 2016; Renault et al., 2017). This process, based on the simple idea that wind stress depends on relative wind speed in a frame of reference moving with the current, rather than absolute wind speed, has consequences in the wind-stress distribution over a mesoscale eddy. The wind stress is increased where the current opposes the wind, and decreased where the current flows in the direction of the wind. This results in a systematic negative wind stress work integrated over an eddy's surface, which extracts kinetic energy (KE) (Dewar & Flierl, 1987), as well as Ekman pumping which induces a negative buoyancy flux that converts available potential energy (APE) into KE (Gaube et al., 2015; Wilder et al., 2022). While these processes were studied in depth in eddying current systems using regional numerical models (Renault, Molemaker, Gula, et al., 2016; Renault et al., 2017), their impact on individual mesoscale eddies remains largely unknown apart from the extremely idealized studies of Dewar and Flierl (1987) and Wilder et al. (2022), which suggest a significant impact of current-feedback on numerical, isolated, idealized eddies. However, observational evidence of the impact of current-feedback on mesoscale eddies are still lacking.

Recently, T. Meunier et al. (2022) applied an empirical method known as the gravest empirical mode method (GEM) (Watts et al., 2001; Sun & Watts, 2001) to reconstruct the daily three-dimensional temperature and salinity structure of all LCRs detached in the GoM between 1993 and 2022. Their method was validated against *in situ* glider observations, and showed a striking accuracy (coefficient of determination R^2 greater than 0.93 between the GEM-reconstructed and the directly observed fields).

In this paper, we take advantage of this validated reconstruction method to estimate the energy decay properties, in time and space, of 40 LCRs detached between 1993 and 2023. Using scatterometer and reanalysis wind products, we also estimate the effect of current feedback on the decay and conversion of the eddies' energy. Beyond a regional study of some particular class of eddy, to the best of our knowledge, this work is the first systematic observation-based statistical study of the energy decay of mesoscale eddies, as well as the first observation-based estimate of the relative impact of wind-current interactions on the decay and conversion of eddies' energy. The results of this study could therefore provide some insight on the processes controlling mesoscale eddy decay in the ocean.

2 Data

This work is largely based on altimeter-derived sea surface height (SSH) observations. We use daily AVISO absolute dynamic topography (ADT) gridded fields. The grid has a $1/4^\circ$ degree resolution and the data is available from January 1st 1993 until now.

We also use nearly 7000 Argo profiles distributed over the entire deep GoM (Fig. 1a). Most of these floats were launched as part of the National Academies of Sciences Understanding Gulf Ocean Systems (UGOS) program.

The main wind product used is IFREMER CERSAT Global Blended Mean Wind Fields, which combines scatterometer observations with ECMWF operational wind analyses. The product is available on a $1/4^\circ$ grid every 6 hours. A 24 hours averaging was performed to coincide with the ADT observations. Detailed information as well as a retrospective study of the product's performance can be found in Desbiolles et al. (2017). Because Scatterometers estimate wind from the sea-state, and the latter depends on relative wind speed rather than absolute wind speed, their wind products are known to retain some signal of the current feedback (Plagge et al., 2012). Although this effect is attenuated by the gridding process, we compared the scatterometer product's results with data from ECMWF's ERA5 reanalysis, which provides estimates of the absolute wind. ERA5 is based on a 4DVAR ensemble data assimilating atmospheric model and is distributed as hourly outputs on a $1/4^\circ$ grid. Here, a 24 hours averaging was also performed. Full details about the methods can be found in Hersbach et al. (2020).

For both wind products, wind stress was computed using the COARE3.5 parameterization (Edson et al., 2013).

3 Methods

3.1 Theoretical background

In this study, we seek to describe the time evolution of the total mechanical energy of individual eddies, which is the three-dimensional integral of energy density over the eddy's volume.

The evolution equation for kinetic energy density ($E_k = \frac{1}{2}\rho|\mathbf{u}|^2$) reads (Gill, 1982):

$$\frac{DE_k}{Dt} + \rho'gw = -\nabla \cdot P'\mathbf{u} + \mathbf{u} \cdot \frac{\partial \boldsymbol{\tau}}{\partial z} + \nabla \cdot \mathbf{K}\nabla E_k + \rho\epsilon, \quad (1)$$

where E_k is kinetic energy, $\frac{D}{Dt}$ is the material derivative, ρ' is density anomaly referenced to a minimum potential energy profile, w is vertical velocity, P' is pressure anomaly, \mathbf{u} is the velocity vector, $\boldsymbol{\tau}$ is the wind stress, z is the vertical coordinate, \mathbf{K} is a diagonal diffusivity coefficient tensor and ϵ is the energy dissipation rate.

The second term on the left-hand side is the buoyancy flux, and is equal to the material rate of change of available potential energy density (Holliday & McIntyre, 1981):

$$\frac{DE_p}{Dt} = \rho'gw, \quad (2)$$

so that the left-hand side of equation (1) represents the material rate of change of total mechanical energy density ($E_m = E_k + E_p$). Still following Holliday and McIntyre (1981), available potential energy density is defined as:

$$E_p = -\int_0^\eta g\tilde{\eta} \frac{\partial \rho_r}{\partial z} (z - \tilde{\eta}) d\tilde{\eta}, \quad (3)$$

where ρ_r is the reference minimum potential energy profile and η is the isopycnal displacement, relative to the reference profile. In this work, we study the effects of the (relative) wind on energy decay and energy conversion, and we compute the buoyancy flux of equation (2) using the non-linear Ekman pumping vertical velocity (Stern, 1965) :

$$w_e = \frac{1}{\rho_0} \nabla \times \left(\frac{\boldsymbol{\tau}}{f + \zeta} \right) \quad (4)$$

Note that computing the non-forced vertical velocity using the Omega equation was also considered, but, since the estimated fields are not necessarily solutions of any equation

149 of motion, and given the relatively low spatial resolution, the omega-derived vertical ve-
 150 locity is essentially noise, with zero-mean vertical velocity.

151 As mentioned above, the wind stress to be considered here is the relative wind stress,
 152 which takes into account the feedback of the current and reads :

$$\boldsymbol{\tau} = \rho_a C_d |\mathbf{u}_a - \alpha \mathbf{u}_g| (\mathbf{u}_a - \alpha \mathbf{u}_g), \quad (5)$$

153 where ρ_a is air density, C_d is the drag coefficient computed using the COARE3.5 param-
 154 eterization (Edson et al., 2013), \mathbf{u}_a is the absolute wind velocity 10 m above the sea sur-
 155 face and \mathbf{u}_g is the velocity of the surface current, computed from the altimetry-derived
 156 SSH using the geostrophic balance assumption. α is a coefficient applied to the current
 157 velocity to account for the feedback of the stress increase/reduction by the current-feedback
 158 through frictional effects, that results in a reduction/increase of the absolute wind speed
 159 (Renault, Molemaker, McWilliams, et al., 2016). We used values of 1 and 0.7, following
 160 empirical results of Renault et al. (2019).

161 We are interested in quantifying the evolution of the total energy (\mathbb{E}_m) transported
 162 by an eddy whose boundary is defined by the closed line \mathcal{C} which encircles the surface
 163 \mathcal{S} :

$$\mathbb{E}_m = \iint_{\mathcal{S}} \int_{-H}^0 E_m dz ds, \quad (6)$$

164 where ds is a surface element and H is the eddy's thickness. We do not make the hy-
 165 pothesis that the boundary \mathcal{C} is a material line. Integrating the left hand side of equa-
 166 tion (1) in its flux form, using the Ostrogradski theorem, the Leibniz theorem, and the
 167 Reynolds transport theorem, we get an exact equation for the evolution of total mechan-
 168 ical energy, under the assumption that the thickness does not vary :

$$\begin{aligned} \frac{d}{dt} \mathbb{E}_m = \int_{-H}^0 \left\{ \underbrace{\oint_{\mathcal{C}} (\mathbf{u}_c - \mathbf{u}) \cdot \mathbf{n} E_m dl}_{(a)} - \underbrace{\oint_{\mathcal{C}} \mathbf{u} \cdot \mathbf{n} P' dl}_{(b)} + \underbrace{\iint_{\mathcal{S}} \mathbf{u} \cdot \frac{\partial \boldsymbol{\tau}}{\partial z} ds}_{(c)} \right. \\ \left. + \underbrace{\oint_{\mathcal{C}} \mathbf{K} \nabla E_k \cdot \mathbf{n} dl}_{(d)} + \underbrace{\iint_{\mathcal{S}} \rho \epsilon ds}_{(e)} \right\} dz \quad (7) \end{aligned}$$

169 The first term on the right hand side represents the energy flux through the eddy's
 170 boundary that is caused by the relative flow in the eddy's moving referential. In the case
 171 of a Lagrangian coherent vortex, the boundary \mathcal{C} is a material line, so that it is exactly
 172 advected by the flow ($\mathbf{u}_c = \mathbf{u}$) and the term vanishes. the second term is the work of
 173 the pressure force. Under the geostrophic approximation, it is null whatever the bound-
 174 ary. The third term is the wind stress work. Since the wind stress is dependent on the
 175 relative wind speed, even an homogeneous wind will exert some work, whose integral over
 176 the eddy's surface will be negative, whatever the vorticity sign (Dewar & Flierl, 1987).
 177 The viscous terms (d) represent all the unresolved (sub-grid scale) advective turbulent
 178 processes that might cause an energy flux through the eddy's boundary (which is only
 179 defined using coarse resolution observations) and the dissipation term (e) is essentially
 180 related to small scale turbulence yielding conversion of mechanical energy to internal en-
 181 ergy.

182 Because we are interested in examining and comparing the energy evolution of a
 183 set of eddies of different sizes, we need to use a normalized metric. The surface-averaged
 184 energy is a convenient variable:

$$\bar{E}_m = \frac{\mathbb{E}_m}{S}. \quad (8)$$

185 Integrating equation (7) with respect to time and dividing by the instantaneous
186 area of the eddy, we get an equation for the surface-averaged energy density.

$$\bar{E}_m(t) = \frac{1}{S} \int_0^t \int_{-H}^0 \{(a) + (b) + (c) + (d) + (e)\} dz d\tau \quad (9)$$

187 Since our purpose is to compute statistical properties of energy decay by ensemble-
188 averaging over all the detached eddies, using the surface-averaged energy density is con-
189 venient. Ensemble averaging using the integrated total energy would introduce a bias
190 by increasing the weight of large eddies in the average. Normalizing total energy by each
191 eddy's area avoids this bias. More interestingly, normalizing energy by the eddy's area
192 also removes the effects of energy loss due to direct loss or gain of area (hence mass), as
193 can happen during filamentation or splitting/merging events. For the sake of concision,
194 in the rest of the paper, the terms KE, APE and TE will be used to designate the sur-
195 face averaged kinetic, potential and total mechanical energy density. When studying the
196 impact of the current-modified wind stress on the eddies' energy, the two variables we
197 will focus on are the surface-averaged, time-integrated wind stress work, normalized by
198 the TE's initial value of each eddy that we will casually refer to as the wind stress work
199 (WSW), and the surface-averaged, time-integrated Ekman buoyancy flux, normalized
200 by the initial value of APE of each eddy, that we will casually refer to as the Ekman buoy-
201 ancy flux (EBF) :

$$\text{WSW}(t) = \frac{1}{\bar{E}_m(0)} \frac{\int_0^t \iint_{\mathcal{S}} \boldsymbol{\tau}(\tilde{t}) \cdot \mathbf{u}_g(\tilde{t}) ds d\tilde{t}}{S(t)}, \quad (10)$$

$$\text{EBF}(t) = \frac{1}{\bar{E}_p(0)} \frac{\int_0^t \int_{-H}^0 \iint_{\mathcal{S}} \rho' g w_e ds dz d\tilde{t}}{S(t)}. \quad (11)$$

203 3.2 The gravest empirical mode method (GEM)

204 To estimate the daily 3D structure of temperature and salinity (hence geostrophic
205 velocity, KE and APE density) from satellite altimetry, we use an empirical method known
206 as the gravest empirical mode projection (GEM) (Watts et al., 2001; Sun & Watts, 2001;
207 T. Meunier et al., 2022). It consists of establishing an empirical relationship between the
208 vertical thermohaline structure of the ocean and the dynamic height to build transfer
209 functions that associate one single value of temperature and salinity for each couple {pressure,
210 SSH}. The procedure used here was used and validated in the Gulf of Mexico and is de-
211 scribed in details in T. Meunier et al. (2022). The mean yearly transfer functions for salin-
212 ity and temperature are shown in Figure 1c and d, respectively : the downward sloping
213 of the isotherms and of the subsurface salinity maximum with increasing SSH, associ-
214 ated with the subtropical underwater (SUW) carried by LCRs is evident. Note that, to
215 account for the seasonality of surface conditions, which affects the accuracy of the three-
216 dimensional reconstruction in the top 200 dbar, the GEM fields were constructed on a
217 monthly basis. An example of APE and KE density cross-section reconstructed using
218 the GEM along with an average LCR's SSH anomaly is shown in Figure 1e and f, respec-
219 tively. APE is concentrated in the core of the eddy, while KE is stronger near the edges,
220 where density gradients are sharper. The APE maximum is 2.5 times larger than the KE
221 maximum and, when integrated over the whole LCR, APE largely dominates over KE
222 (T. Meunier et al., 2022).

223

3.3 Eddies' edge definition

224

225

226

227

228

229

230

231

232

233

234

235

236

237

238

239

240

241

242

243

244

245

246

247

248

249

250

251

252

253

254

255

256

In this work, we aim to follow the whole LCR, and not only its coherent part, which is usually confined to a small portion of the core (Beron-Vera et al., 2018; Andrade-Canto et al., 2020). Hence, rather than tracking so called Lagrangian coherent vortices (Haller & Beron-Vera, 2013; Beron-Vera et al., 2013), the eddy as we wish to track it should be defined as a compact rotating body of water detached from the LC, regardless of its *a priori* conservation properties. The detection and tracking method is based on ADT. First we define the LC's edge as the smallest-value ADT contour linking the Yucatan channel and the Florida strait. This contour usually encloses closed ADT contours, which are the signature of unborn LCRs. We define LCR detachment as the instant at which none of the closed contours remain enclosed within the LC anymore. Once detached, to define the LCR's boundary, we use a mixed Eulerian-Lagrangian procedure : at $t=0$ (detachment date), we initialize a cluster of virtual Lagrangian particles within the outermost closed SSH contour, which coincides with the boundary of the water mass detached from the LC. These particles are distributed on a $1\text{ km}\times 1\text{ km}$ regular grid. They are then integrated in the geostrophic surface velocity field inferred from the altimetry product, using a fourth-order Runge-Kutta scheme (Butcher, 1996). The particle concentration is then computed and interpolated on a regular $1/48^\circ$ grid. The LCR's edge is defined as the concentration contour with the original value at $t=0$, that is, the closed isopleth that encloses a compact surface of constant concentration equal to the original concentration. A sequence of particle concentration maps during the drift of LCR Poseidon in April and November 2016 is shown on figure 1g and h. The edge contour based on the concentration criterion is compared to two other Eulerian criteria : the Maximum velocity contour and the last closed SSH contour. While particle loss through filamentation of the eddy is evident, concentration within the eddy's boundary remain largely homogeneous. It is important to note that, while the method is based on Lagrangian particles integration, it does not belong to the class of *Lagrangian methods*, that seek coherent eddy boundaries, such as the null geodesics rings of Haller and Beron-Vera (2013) and Beron-Vera et al. (2018). Here, the boundary does not ensure the coherence of the eddy, in the sense that tracer conservation is not guaranteed (and our detected eddies actually do loose tracer). However, contrary to Lagrangian Coherent Vortices detected using proper *Lagrangian methods*, this method allows us to follow the entire body of water detached from the LC, and not only a small fragment of it. The initial boundaries of all eddies are shown in Figure 1b, where the SSH at the eddies' centers is color-coded.

257

4 Results

258

259

260

261

262

263

264

265

266

267

268

269

270

271

272

273

274

Individual trajectories of the 40 LCRs are shown on Figure 2a. TE, normalized by the initial values at the time of detachment, is color-coded. While a few LCRs maintain high levels of energy ($>80\%$) past the Campeche bank, west of 93°W , the vast majority start losing energy soon in their life cycle in the eastern GoM. The ensemble average of normalized TE for all LCRs is shown in Figures 2b. The circles' size represents the average diameter of LCRs during their drift. After 200 days, the average TE left in the eddies is only 26 % of the initial value at detachment. This value is of 21 and 28 % for KE and APE, respectively (not shown).

The evolution of the mean KE, APE and TE (non-normalized by initial values) is shown against time and longitude on figure 2c. The 95% confidence interval, computed using the bootstrap method, is shown as the light shaded areas. APE largely dominates over KE during the entire eddies' life cycle. On average, both KE and APE start decaying right from the first days after detachment and keep on decaying continuously with time until 200 days, resulting in a similar decay of TE. The average halving time for KE, APE and TE is of 101 days, 120 days, and 117 days, respectively. Looking at the longitude-dependence of energy, a similar pattern appears : APE and KE start decaying in the eastern basin near 88.5°W and decay continuously across the entire GoM. The halving lon-

275 gitude is of 91°W for KE and 91.6°W for APE and TE. The energy decay rates (Fig-
 276 ure 2d) not only confirm that energy loss occurs all along the eddies' drift through the
 277 GoM, but also that LCRs lose APE (and TE) at a faster rate in the eastern GoM, dur-
 278 ing the first month of their life cycle. KE does not exhibit this increased decay rate in
 279 the eastern basin, and decays regularly all along the eddies life cycle.

280 Since previous works have pointed out some critical longitude ($\approx 92\text{-}93^\circ\text{W}$) where
 281 eddies seem to decay at a faster rate, mostly because of instability and eddy-splitting
 282 (direct loss of mass; see Lipphardt et al. (2008) and references therein), we also inves-
 283 tigated the evolution of the total LCRs energy (the energy density integrated over the
 284 full eddy's surface and not the energy per unit area discussed above) as well as the evo-
 285 lution of the eddies area, which would clearly indicate regions of more frequent splitting.
 286 The surface integrated KE, APE and TE, normalized by their initial values and ensemble-
 287 averaged are shown against time and longitude in Figures 2e and f, respectively. As for
 288 the surface-averaged KE, TE and APE, the surface integrated KE, TE and APE smoothly
 289 and regularly decay with time during the whole LCRs life cycle. Similarly, the decay against
 290 longitude shows no obvious discontinuity, except for a slightly faster decay between 90
 291 and 91°W . The evolution of the ensemble-averaged LCRs areas against time and lon-
 292 gitude shows the same regular decay, without any evident discontinuity.

293 Equation (7) shows that for a mesoscale geostrophic eddy, where the work of the
 294 pressure force is negligible, TE can only decay through the action of wind stress work,
 295 an energy flux through the boundary, and diffusivity. As mentioned above, the energy
 296 flux through the boundary is impossible to estimate, since the boundary's velocity is un-
 297 definable (because it is not defined by a series of material points, or material line), and
 298 the diffusive term can not be estimated with satellite altimetry and Argo data only. On
 299 the other hand, the effects of wind stress work can be assessed using wind observations.
 300 Similarly, the decay of APE is directly linked to buoyancy fluxes (Equation 3), and while
 301 the vertical velocity can not be fully estimated, we still can estimate the contribution
 302 of Ekman pumping to it (Equation 4). In other words, while this work does not allow
 303 for a full budget of the energy equation, the effects of relative wind stress can be assessed
 304 effectively. Figure 2g compares the average evolution of TE (normalized by initial val-
 305 ues) to the effects of wind stress work for 4 different wind stress parametrization : ab-
 306 solute wind stress obtained from scatterometer products (SCAT abs), relative wind stress
 307 obtained from scatterometer products and computed by removing the full current ve-
 308 locity from the absolute wind value (SCAT rel), relative wind stress obtained from the
 309 ERA5 reanalysis and computed by removing the full current velocity from the absolute
 310 wind value (ERA rel), and relative wind stress obtained from scatterometer products and
 311 computed by removing 70 % of the current velocity to the absolute wind value (SCAT
 312 rel07). Relative wind stress work appears to contribute to the decay of the LCRs' TE,
 313 with an average of 18% and 15% of the original TE extracted when using Scatterome-
 314 ter and ERA5 wind products, respectively. This corresponds to respectively a quarter
 315 and a fifth of the energy lost by LCRs in 200 days. When using Renault et al. (2019)'s
 316 parameterization which uses a current velocity reduced by 30% to compute relative wind
 317 stress (SCAT rel07), we find that, on average, wind stress work then only accounts for
 318 about 10 % of the TE loss in LCRs. In all three cases, energy decay through wind stress
 319 work is faster in the beginning of the LCR's life cycle, and after about 120 days, wind
 320 stress work does not extract energy any more. For comparison, the work of the absolute
 321 wind was also computed. Surprisingly, it represents an energy source for LCRs with an
 322 average increase of the original TE by about 20% after 200 days. This shows that the
 323 mean spatial distribution of absolute wind in the GoM tends to increase LCRs energy,
 324 showing that the energy sink is really related to wind-current interactions.

325 Time evolution of APE is compared to the effects of Ekman buoyancy fluxes in fig-
 326 ure 2h. The wind parameterizations shown are the same as for Figure 2g. The close co-
 327 incidence of the decay of APE and that expected from Ekman buoyancy fluxes computed
 328 from scatterometer-derived relative wind stress is striking. It suggests that Ekman buoy-
 329 ancy fluxes might account for the whole observed APE decay. Using ERA5 relative wind

330 stress, we find that Ekman buoyancy flux accounts for a slightly reduced part of the APE
 331 decay (70 % of the APE loss after 200 days), and using the reduced current parameter-
 332 ization for relative wind stress computation (SCAT abs07), Ekman buoyancy flux ac-
 333 counts for about 65% of the total APE loss in 200 days. Using absolute wind stress, we
 334 find that Ekman buoyancy flux corresponds to an APE increase of nearly 20% during
 335 the first 170 days, followed by a small decrease in the last 30 days.

336 5 Discussion and conclusion

337 Using an observation-based method, we assessed the statistical properties of the
 338 energy decay of all LCRs detached since 1993. To the best of our knowledge, this is the
 339 first time such statistics on the energy decay of mesoscale eddies are obtained anywhere
 340 in the World ocean based on an observations.

341 We showed that LCRs' energy decay is a fast process occurring continuously dur-
 342 ing the whole eddies' life cycles. This observation is in contradiction with the commonly
 343 accepted idea that LCRs steadily drift through the GoM, retaining their hydrographic
 344 properties until they collapse against the western platform, as explicitly shown in the
 345 numerical simulations of Romanou et al. (2004), and suggested in a number of other nu-
 346 merical studies listed in Lipphardt et al. (2008) (Sturges et al., 1993; Dietrich et al., 1997;
 347 Kantha et al., 2005). However, it should be pointed out that our results do not contra-
 348 dict the idea of an *eddy graveyard*, but clearly show that the decay of LCRs does not hap-
 349 pen only there, but starts right from the first month after detachment from the LC and
 350 continues all along their life cycle. As they reach the so-called graveyard, LCRs are al-
 351 ready old and weak eddies that have typically lost over 3/4 of their energy. Topographic
 352 effects in the western basin can therefore not be considered a major cause of LCRs de-
 353 cay, but rather the ultimate process dispersing their remnants. Moreover, the energy de-
 354 cay rate was shown to be faster in the eastern basin soon after detachment than in the
 355 western basin, and the halving longitude is found as far East as 91.5°W.

356 Our results also contradict another long-standing claim that there exists some crit-
 357 ical longitude in the GoM, between 92 and 93°W, beyond which LCRs suddenly decay
 358 at a fast rate, mostly through low wavenumber instability (the observed elliptization of
 359 the eddies seems consistent with the development of an azimuthal mode 2 vortex Rossby
 360 wave) yielding vortex-splitting (Hamilton et al., 1999; Vukovich, 2007; Lipphardt et al.,
 361 2008). Although we acknowledge that LCRs might become unstable, loose coherence or
 362 split as directly observed by Biggs et al. (1996), so that increased decay rate might oc-
 363 casionally occur in the central basin, our results show no sign of a critical longitude be-
 364 tween 92 and 93 °W (nor anywhere) where LCRs loose mass or energy at a faster rate,
 365 and the decay of the eddies' area and surface-integrated KE, APE and TE is a gradual
 366 process occurring all through their life cycles.

367 Beyond the description of the decay of energy in LCRs, we also investigated the
 368 possible role of wind-current feedback on that decay. We showed that the effect of rel-
 369 ative wind stress work is non-negligible, but likely not a leading order mechanism in the
 370 decay of kinetic energy (and total mechanical energy) as it accounts for 25 and 20 % of
 371 the total energy loss in 200 days when using scatterometer and ERA5 wind fields, re-
 372 spectively. When using Renault et al. (2019)'s parameterization to account for the dimin-
 373 ution of absolute wind when the current opposes the wind (and *vice versa*) (by reducing
 374 the current velocity by 30 % when computing relative wind stress), we found that wind
 375 stress work then only accounts for 10 % of the total energy loss in 200 days.

376 However, the impact of current-feedback was shown to be important for the decay
 377 of APE, which would be entirely driven by Ekman buoyancy flux when using relative
 378 wind stress computed from scatterometer data. Beyond this striking result, the control
 379 of APE loss by Ekman buoyancy flux has implications on the decay of KE. Buoyancy
 380 flux does not extract TE: it converts APE to KE (it is often referred to as the baroclinic
 381 conversion term), which means that all along the LCRs life cycle, KE is fueled by this
 382 conversion. Given the modest role of wind stress work, this means that some other pro-

cesses, such as turbulent diffusivity at the edges of the eddies (subgrid-scale advective processes that are unresolved by the altimetry grid) might be important in the decay of LCRs' TE through the decay of KE.

Of course, our study does not allow estimation of the impact of direct energy flux through the eddies' boundary which is related to the fact that the edges we consider are not material lines (term (a) in equation 7). This is clearly a caveat of not using Lagrangian coherent boundaries, which would ensure the flux term to be zero, and would allow us to estimate the diffusive term as it would become the only unknown of Equation (7). The choice not to use such Lagrangian metrics was motivated by the need to estimate the evolution of the full detached patch of LC water, and not only a small piece of its core. In particular, relative wind stress work becomes important near the edge of the eddies, where the velocity is maximum, while long-horizon coherent LCRs usually exclude this peripheral part. However, working with three-dimensional Lagrangian objective eddy framing (Beron-Vera et al., 2013; Haller & Beron-Vera, 2013) would be complementary to this study. Although it would only allow to estimate the properties and fate of the inner core of LCRs, it could allow to study more accurately the impact of Ekman buoyancy fluxes in baroclinic conversion. Such study is currently in progress.

Note that, while this study is focused on the GoM, similar processes are expected to occur in other warm-core rings (e.g. Agulhas rings, Gulf stream rings, Mozambic channel rings, North Brazil Current rings, Kuroshio rings etc.) and a similar study, dedicated to the decay of Agulhas rings is also in progress.

6 Open Research

All data used in this study are publicly available. The gridded scatterometer wind product and the absolute dynamic topography SSH product are available from Copernicus (<https://data.marine.copernicus.eu>). Direct link to the wind product dataset is also available at <https://www.pigma.org/geonetwork/srv/api/records/85c907d3-98fc-4ce7-b7e4-7332aa3fe660>. Direct link to the ADT product is also available at https://data.marine.copernicus.eu/product/SEALEVEL_GLO_PHY_CLIMATE_L4_MY_008_057/download. Data is available after users create a Copernicus account. Argo data are available from any data assembly center (e.g. <https://dataselection.euro-argo.eu/>), specifying the geographical limits of $[-99 -80]^{\circ}W$ and $[17 31]^{\circ}N$.

Acknowledgments

The authors are grateful to Amala Mahadevan, Mike Spall, Lionel Renault and Xavier Carton for their useful suggestions and comments. This work is part of the LC-floats and UGOS3 projects, funded by the US National Academy of Sciences through the Understanding Gulf Ocean Systems grants 2000010488 and 200013145.

References

- Andrade-Canto, F., Karrasch, D., & Beron-Vera, F. J. (2020, November). Genesis, evolution, and apocalypse of Loop Current rings. *Physics of Fluids*, *32*(11), 116603. doi: 10.1063/5.0030094
- Armi, L., Hebert, D., Oakey, N., Price, J. F., Richardson, P. L., Thomas Rossby, H., & Ruddick, B. (1989, March). Two Years in the Life of a Mediterranean Salt Lens. *Journal of Physical Oceanography*, *19*(3), 354-370. doi: 10.1175/1520-0485(1989)019<0354:TYITLO>2.0.CO;2
- Beal, L. r., De Ruijter, W. r. r., Biastoch, A., Zahn, R., & SCOR/WCRP/IAPSO Working Group 136. (2011, April). On the role of the Agulhas system in ocean circulation and climate. , *472*(7344), 429-436. doi: 10.1038/nature09983
- Beron-Vera, F. J., Olascoaga, M. J., Wang, Y., Triñanes, J., & Pérez-Brunius, P. (2018, July). Enduring Lagrangian coherence of a Loop Current ring as-

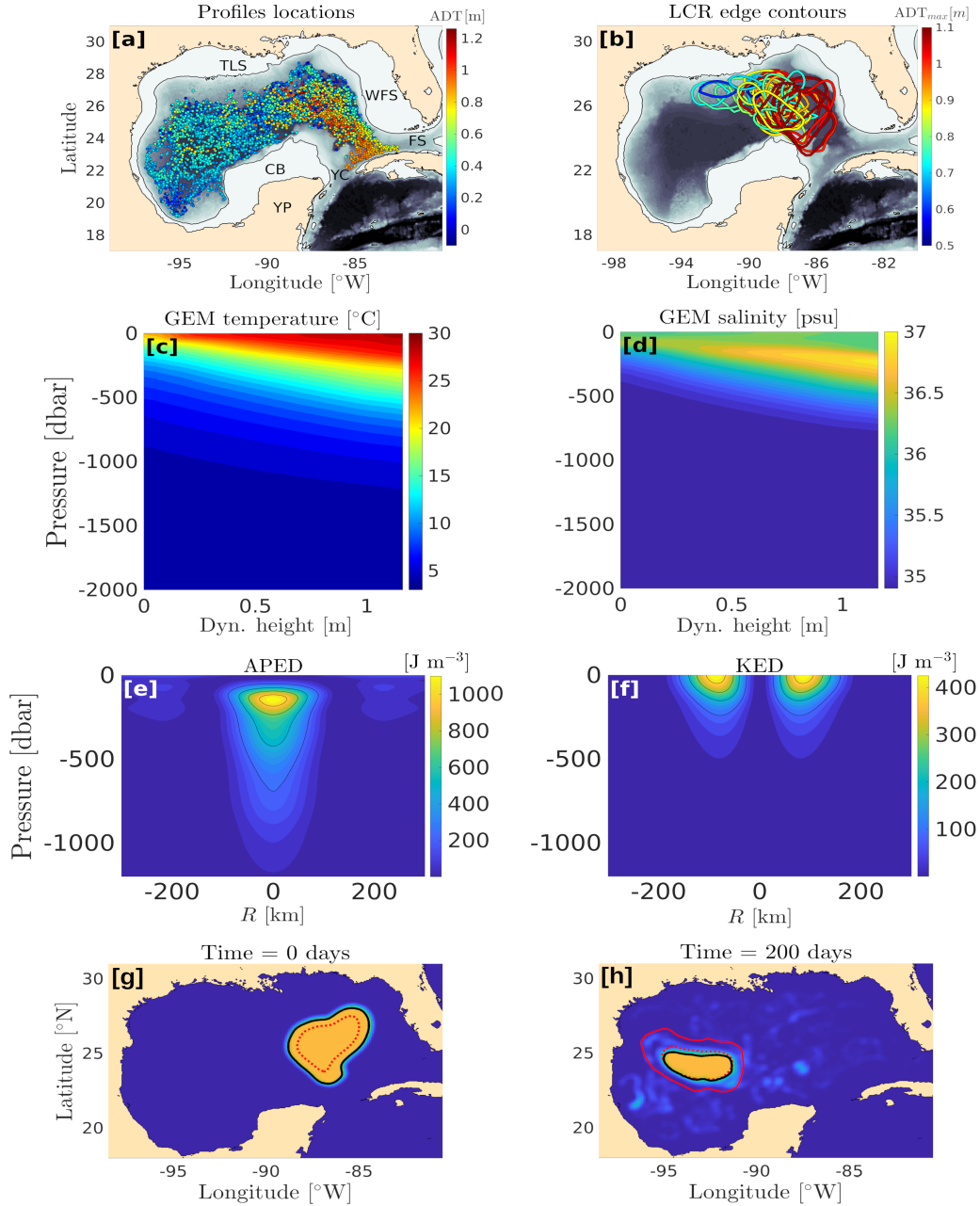


Figure 1. a: Location of the ARGO profiles used to build the Gravest Empirical Modes (GEM) for the Gulf of Mexico (GoM). The color code represents the local Absolute Dynamic Topography (ADT). The names of the GoM’s main topographic features are indicated. YC stands for Yucatan channel, FS stands for Florida strait, WFS stands for West Florida shelf, CB stands for Campeche bank, YP stands for Yucatan peninsula, and TLS stands for Texas-Louisiana shelf. b: Edge contours on the first day after detachment for all the Loop Current Rings (LCR) detached between 1993 and 2023. The color code represents ADT at the center of the eddy. c: GEM transfer function for temperature. The x-axis is dynamic height, the y-axis is pressure, and the color map is temperature. d: Same as (c) for salinity. e: Available potential energy density section across an average LCR reconstructed using the GEM method. f: same as (e) for kinetic energy density. g: Initial particle concentration in Loop Current Ring Poseidon on detachment date. The plain and dashed red lines represent the last closed ADT contour and the maximum velocity contour, respectively. Normalized passive tracer concentration is color-coded (yellow is 1 and dark blue is zero). The concentration-based edge contour of Poseidon is materialized as a thick black line. h: Same as (g) after 200 days—11—

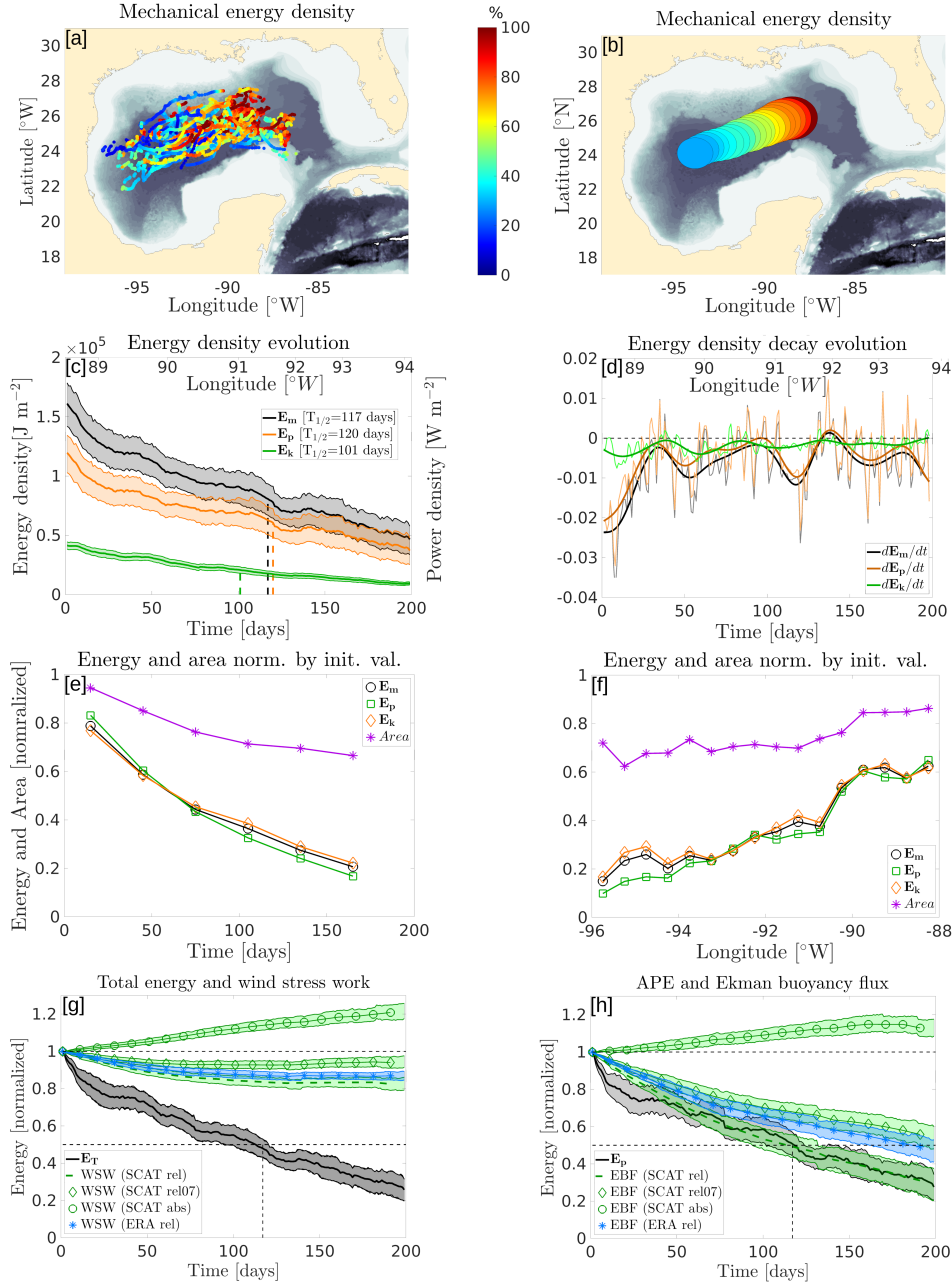


Figure 2. a: Trajectories of the center of the 40 Loop Current Rings (LCR). Total mechanical energy (TE) normalized by its initial value is color-coded. b: Ensemble-averaged TE normalized by its initial value. The position and diameter of the circles represent the average position and size of the LCRs. c: Time evolution of the average energy density. The black, orange and green lines represent total mechanical energy (TE), available potential energy (APE), and kinetic energy (KE), respectively. The light shaded areas around the lines represent the 95% confidence interval. The vertical dashed lines represent the energy halving time. The average longitude corresponding to the time is indicated on the top x-axis. d: Time evolution of the ensemble averaged rate of change of energy density (time derivative of energy density). The smooth dark thick lines represent the 30-days low pass filtered values, while the thin light lines represent the raw results. The color code is the same as in panel (c). e: Ensemble average of the non-surface-averaged KE (orange diamonds), TE (black circles) and APE (green squares) and eddy's area (purple stars) normalized by their initial values against time. f: Same as (e) against longitude. g: Energy extraction by the effects of wind stress work. The dashed line represents wind stress work computed from the scatterometer data. The green diamonds represent wind stress work computed by reducing the current by a factor of a 0.7 when computing relative wind. The red circles represent the effect of wind stress work computed using the absolute wind stress. The blue stars represent the effect of wind stress work computed using the ERA5 reanalysis. Time evolution of the TE is indicated as a black line. h: Energy conversion by the effect of the Ekman buoyancy flux. The Color code is the same as in panel (g). Time evolution of APE is indicated as the black line.

- 432 sessed using independent observations. *Scientific Reports*, 8, 11275. doi:
433 10.1038/s41598-018-29582-5
- 434 Beron-Vera, F. J., Wang, Y., Olascoaga, M. J., Goni, G. J., & Haller, G. (2013,
435 July). Objective Detection of Oceanic Eddies and the Agulhas Leak-
436 age. *Journal of Physical Oceanography*, 43(7), 1426-1438. doi: 10.1175/
437 JPO-D-12-0171.1
- 438 Biastoch, A., Böning, C. W., & Lutjeharms, J. R. E. (2008, November). Agulhas
439 leakage dynamics affects decadal variability in Atlantic overturning circulation.
440 , 456(7221), 489-492. doi: 10.1038/nature07426
- 441 Biggs, D. C. (1992, February). Nutrients, plankton, and productivity in a
442 warm-core ring in the western Gulf of Mexico. , 97(C2), 2143-2154. doi:
443 10.1029/90JC02020
- 444 Biggs, D. C., Fargion, G. S., Hamilton, P., & Leben, R. R. (1996, September).
445 Cleavage of a Gulf of Mexico Loop Current eddy by a deep water cyclone. ,
446 101(C9), 20629-20642. doi: 10.1029/96JC01078
- 447 Brammigan, L., Marshall, D. P., Naveira Garabato, A. C., Nurser, A. J. G., & Kaiser,
448 J. (2017, December). Submesoscale Instabilities in Mesoscale Eddies. *Journal*
449 *of Physical Oceanography*, 47(12), 3061-3085. doi: 10.1175/JPO-D-16-0178.1
- 450 Butcher, J. C. (1996). A history of runge-kutta methods. *Applied numerical mathe-*
451 *matics*, 20(3), 247-260.
- 452 Candela, J., Sheinbaum, J., Ochoa, J., Badan, A., & Leben, R. (2002, November).
453 The potential vorticity flux through the Yucatan Channel and the Loop Cur-
454 rent in the Gulf of Mexico. , 29(22), 2059. doi: 10.1029/2002GL015587
- 455 de Marez, C., Meunier, T., Morvan, M., L'Hégaret, P., & Carton, X. (2020, Febru-
456 ary). Study of the stability of a large realistic cyclonic eddy. *Ocean Modelling*,
457 146, 101540. doi: 10.1016/j.ocemod.2019.101540
- 458 Desbiolles, F., Bentamy, A., Blanke, B., Roy, C., Mestas-Nuñez, A. M., Grodsky,
459 S. A., ... Maes, C. (2017, April). Two decades [1992-2012] of surface wind
460 analyses based on satellite scatterometer observations. *Journal of Marine*
461 *Systems*, 168, 38-56. doi: 10.1016/j.jmarsys.2017.01.003
- 462 Dewar, W. K. (1987, December). Ventilating Warm Rings: Theory and Energet-
463 ics. *Journal of Physical Oceanography*, 17(12), 2219-2231. doi: 10.1175/1520
464 -0485(1987)017<2219:VWRTAE>2.0.CO;2
- 465 Dewar, W. K., & Flierl, G. R. (1987, October). Some Effects of the Wind
466 on Rings. *Journal of Physical Oceanography*, 17(10), 1653-1667. doi:
467 10.1175/1520-0485(1987)017(1653:SEOTWO)2.0.CO;2
- 468 Dietrich, D. E., Lin, C. A., Mestas-Nunez, A., & Ko, D. S. (1997, January). A
469 high resolution numerical study of Gulf of Mexico fronts and eddies. *Meteorol-*
470 *ogy and Atmospheric Physics*, 64(3-4), 187-201. doi: 10.1007/BF01029692
- 471 Donohue, K. A., Watts, D. R., Hamilton, P., Leben, R., & Kennelly, M. (2016, De-
472 cember). Loop Current Eddy formation and baroclinic instability. *Dynamics of*
473 *Atmospheres and Oceans*, 76, 195-216. doi: 10.1016/j.dynatmoce.2016.01.004
- 474 Duhaut, T. H. A., & Straub, D. N. (2006, January). Wind Stress Dependence
475 on Ocean Surface Velocity: Implications for Mechanical Energy Input to
476 Ocean Circulation. *Journal of Physical Oceanography*, 36(2), 202. doi:
477 10.1175/JPO2842.1
- 478 Edson, J. B., Jampana, V., Weller, R. A., Bigorre, S. P., Plueddemann, A. J.,
479 Fairall, C. W., ... Hersbach, H. (2013, August). On the Exchange of Mo-
480 mentum over the Open Ocean. *Journal of Physical Oceanography*, 43(8),
481 1589-1610. doi: 10.1175/JPO-D-12-0173.1
- 482 Elliott, B. A. (1982, November). Anticyclonic Rings in the Gulf of Mex-
483 ico. *Journal of Physical Oceanography*, 12(11), 1292-1309. doi: 10.1175/
484 1520-0485(1982)012(1292:ARITGO)2.0.CO;2
- 485 Forristall, G. Z., Schaudt, K. J., & Cooper, C. K. (1992, February). Evolution and
486 kinematics of a loop current eddy in the Gulf of Mexico during 1985. , 97(C2),

- 487 2173-2184. doi: 10.1029/91JC02905
- 488 Gaube, P., Chelton, D. B., Samelson, R. M., Schlax, M. G., & O'Neill, L. W.
489 (2015, January). Satellite Observations of Mesoscale Eddy-Induced Ek-
490 man Pumping. *Journal of Physical Oceanography*, *45*(1), 104-132. doi:
491 10.1175/JPO-D-14-0032.1
- 492 Haller, G., & Beron-Vera, F. J. (2013, September). Coherent Lagrangian vortices:
493 the black holes of turbulence. *Journal of Fluid Mechanics*, *731*, R4. doi: 10
494 .1017/jfm.2013.391
- 495 Hamilton, P., Fargion, G. S., & Biggs, D. C. (1999, June). Loop Current Eddy Paths
496 in the Western Gulf of Mexico. *Journal of Physical Oceanography*, *29*(6), 1180-
497 1207. doi: 10.1175/1520-0485(1999)029<1180:LCEPIT>2.0.CO;2
- 498 Hamilton, P., Leben, R., Bower, A., Furey, H., & Pérez-Brunius, P. (2018, April).
499 Hydrography of the Gulf of Mexico Using Autonomous Floats. *Journal of*
500 *Physical Oceanography*, *48*(4), 773-794. doi: 10.1175/JPO-D-17-0205.1
- 501 Hersbach, H., Bell, B., Berrisford, P., Hirahara, S., Horányi, A., Muñoz-Sabater,
502 J., ... Thépaut, J.-N. (2020, July). The ERA5 global reanalysis. *Quar-*
503 *terly Journal of the Royal Meteorological Society*, *146*(730), 1999-2049. doi:
504 10.1002/qj.3803
- 505 Holliday, D., & McIntyre, M. E. (1981, June). On potential energy density in an in-
506 compressible, stratified fluid. *Journal of Fluid Mechanics*, *107*, 221-225. doi:
507 10.1017/S0022112081001742
- 508 Jaimes, B., Shay, L. K., & Brewster, J. K. (2016, December). Observed air-
509 sea interactions in tropical cyclone Isaac over Loop Current mesoscale
510 eddy features. *Dynamics of Atmospheres and Oceans*, *76*, 306-324. doi:
511 10.1016/j.dynatmoce.2016.03.001
- 512 Jouanno, J., Ochoa, J., Pallàs-Sanz, E., Sheinbaum, J., Andrade-Canto, F., Can-
513 dela, J., & Molines, J.-M. (2016, November). Loop Current Frontal
514 Eddies: Formation along the Campeche Bank and Impact of Coastally
515 Trapped Waves. *Journal of Physical Oceanography*, *46*(11), 3339-3363. doi:
516 10.1175/JPO-D-16-0052.1
- 517 Joyce, T. M., Toole, J. M., Klein, P., & Thomas, L. N. (2013, April). A near-inertial
518 mode observed within a Gulf Stream warm-core ring. *Journal of Geophysical*
519 *Research (Oceans)*, *118*(4), 1797-1806. doi: 10.1002/jgrc.20141
- 520 Kantha, L., Choi, J.-K., Schaudt, K. J., & Cooper, C. K. (2005, January). A
521 regional data-assimilative model for operational use in the Gulf of Mexico.
522 *Washington DC American Geophysical Union Geophysical Monograph Series*,
523 *161*, 165-180. doi: 10.1029/161GM14
- 524 Kunze, E. (1986, August). The Mean and Near-Inertial Velocity Fields in a Warm-
525 Core Ring. *Journal of Physical Oceanography*, *16*(8), 1444-1461. doi: 10.1175/
526 1520-0485(1986)016<1444:TMANIV>2.0.CO;2
- 527 Leben, R. R. (2005, January). Altimeter-derived loop current metrics. *Washington*
528 *DC American Geophysical Union Geophysical Monograph Series*, *161*, 181-201.
529 doi: 10.1029/161GM15
- 530 Le Hénaff, M., Kourafalou, V. H., Androulidakis, Y., Ntaganou, N., & Kang, H.
531 (2023). Influence of the caribbean sea eddy field on loop current predictions.
532 *Frontiers in Marine Science*, *10*, 1129402.
- 533 Lipphardt, B. L., Poje, A. C., Kirwan, A. D., Kantha, L., & Zweng, M. (2008).
534 Death of three loop current rings. *Journal of Marine Research*, *66*(1), 25-60.
- 535 Lugo-Fernández, A., Leben, R. R., & Hall, C. A. (2016, December). Kine-
536 matic metrics of the Loop Current in the Gulf of Mexico from satellite
537 altimetry. *Dynamics of Atmospheres and Oceans*, *76*, 268-282. doi:
538 10.1016/j.dynatmoce.2016.01.002
- 539 Mariotti, A., Legras, B., & Dritschel, D. G. (1994, December). Vortex stripping and
540 the erosion of coherent structures in two-dimensional flows. *Physics of Fluids*,
541 *6*(12), 3954-3962. doi: 10.1063/1.868385

- 542 Marsh, R., Hazeleger, W., Yool, A., & Rohling, E. J. (2007, February). Stability of
543 the thermohaline circulation under millennial CO₂ forcing and two alternative
544 controls on Atlantic salinity. , *34*(3), L03605. doi: 10.1029/2006GL027815
- 545 Meunier, Ménesguen, C., Schopp, R., & Le Gentil, S. (2015). Tracer stirring around
546 a meddy: The formation of layering. *Journal of Physical Oceanography*, *45*(2),
547 407–423.
- 548 Meunier, T., Pérez-Brunius, P., & Bower, A. (2022, August). Reconstructing the
549 Three-Dimensional Structure of Loop Current Rings from Satellite Altime-
550 try and In Situ Data Using the Gravest Empirical Modes Method. *Remote*
551 *Sensing*, *14*(17), 4174. doi: 10.3390/rs14174174
- 552 Meunier, T., Sheinbaum, J., Pallàs-Sanz, E., Tenreiro, M., Ochoa, J., Ruiz-Angulo,
553 A., . . . de Marez, C. (2020, February). Heat Content Anomaly and Decay
554 of Warm-Core Rings: the Case of the Gulf of Mexico. , *47*(3), e85600. doi:
555 10.1029/2019GL085600
- 556 Middleton, L., Fine, E. C., MacKinnon, J. A., Alford, M. H., & Taylor, J. R. (2021,
557 August). Estimating Dissipation Rates Associated With Double Diffusion. ,
558 *48*(15), e92779. doi: 10.1029/2021GL092779
- 559 Molina, M. J., Timmer, R. P., & Allen, J. T. (2016, December). Importance of
560 the Gulf of Mexico as a climate driver for U.S. severe thunderstorm activity. ,
561 *43*(23), 12,295-12,304. doi: 10.1002/2016GL071603
- 562 Oey, L. Y., Lee, H. C., & Schmitz, W. J. (2003, October). Effects of winds and
563 Caribbean eddies on the frequency of Loop Current eddy shedding: A numer-
564 ical model study. *Journal of Geophysical Research (Oceans)*, *108*(C10), 3324.
565 doi: 10.1029/2002JC001698
- 566 Pérez, J. G. C., Pallàs-Sanz, E., Tenreiro, M., Meunier, T., Jouanno, J., & Ruiz-
567 Angulo, A. (2022, April). Overturning Instabilities Across a Warm Core Ring
568 From Glider Observations. *Journal of Geophysical Research (Oceans)*, *127*(4),
569 e2021JC017527. doi: 10.1029/2021JC017527
- 570 Plagge, A. M., Vandemark, D., & Chapron, B. (2012, December). Examining the
571 Impact of Surface Currents on Satellite Scatterometer and Altimeter Ocean
572 Winds. *Journal of Atmospheric and Oceanic Technology*, *29*(12), 1776-1793.
573 doi: 10.1175/JTECH-D-12-00017.1
- 574 Polzin, K. L. (2008, January). Mesoscale Eddy-Internal Wave Coupling. Part
575 I: Symmetry, Wave Capture, and Results from the Mid-Ocean Dynam-
576 ics Experiment. *Journal of Physical Oceanography*, *38*(11), 2556. doi:
577 10.1175/2008JPO3666.1
- 578 Renault, L., Marchesiello, P., Masson, S., & McWilliams, J. C. (2019, March).
579 Remarkable Control of Western Boundary Currents by Eddy Killing, a
580 Mechanical Air-Sea Coupling Process. , *46*(5), 2743-2751. doi: 10.1029/
581 2018GL081211
- 582 Renault, L., McWilliams, J. C., & Penven, P. (2017, August). Modulation of the Ag-
583 ulhas Current Retroreflection and Leakage by Oceanic Current Interaction with
584 the Atmosphere in Coupled Simulations. *Journal of Physical Oceanography*,
585 *47*(8), 2077-2100. doi: 10.1175/JPO-D-16-0168.1
- 586 Renault, L., Molemaker, M. J., Gula, J., Masson, S., & McWilliams, J. C. (2016,
587 November). Control and Stabilization of the Gulf Stream by Oceanic Current
588 Interaction with the Atmosphere. *Journal of Physical Oceanography*, *46*(11),
589 3439-3453. doi: 10.1175/JPO-D-16-0115.1
- 590 Renault, L., Molemaker, M. J., McWilliams, J. C., Shchepetkin, A. F., Lemarié, F.,
591 Chelton, D., . . . Hall, A. (2016, June). Modulation of Wind Work by Oceanic
592 Current Interaction with the Atmosphere. *Journal of Physical Oceanography*,
593 *46*(6), 1685-1704. doi: 10.1175/JPO-D-15-0232.1
- 594 Romanou, A., Chassignet, E. P., & Sturges, W. (2004, January). Gulf of Mexico
595 circulation within a high-resolution numerical simulation of the North Atlantic
596 Ocean. *Journal of Geophysical Research (Oceans)*, *109*(C1), C01003. doi:

- 597 10.1029/2003JC001770
598 Schmitt, R. W., Lueck, R. G., & Joyce, T. M. (1986, November). Fine- and mi-
599 crostructure at the edge of a warm-core ring. *Deep Sea Research A*, *33*(11-12),
600 1665-1689. doi: 10.1016/0198-0149(86)90073-7
- 601 Shay, L. K., Goni, G. J., & Black, P. G. (2000). Effects of a warm oceanic feature on
602 hurricane opal. *Mon. Weather Rev.*, *128*, 1366-1383.
- 603 Stern, M. E. (1965, January). Interaction of a uniform wind stress with a
604 geostrophic vortex. *Deep Sea Research A*, *12*(3), 355-367. doi: 10.1016/
605 0011-7471(65)90007-0
- 606 Sturges, W., Evans, J. C., Welsh, S., & Holland, W. (1993, February). Separation
607 of Warm-Core Rings in the Gulf of Mexico. *Journal of Physical Oceanography*,
608 *23*(2), 250-268. doi: 10.1175/1520-0485(1993)023<0250:SOWCRI>2.0.CO;2
- 609 Sun, C., & Watts, D. R. (2001, February). A circumpolar gravest empirical
610 mode for the Southern Ocean hydrography. , *106*(C2), 2833-2855. doi:
611 10.1029/2000JC900112
- 612 Tedesco, P., Gula, J., Ménesguen, C., Penven, P., & Krug, M. (2019, Novem-
613 ber). Generation of Submesoscale Frontal Eddies in the Agulhas Cur-
614 rent. *Journal of Geophysical Research (Oceans)*, *124*(11), 7606-7625. doi:
615 10.1029/2019JC015229
- 616 Vidal, V. M. V., Vidal, F. V., Hernández, A. F., Meza, E., & Zambrano, L. (1994).
617 Winter water mass distributions in the western gulf of mexico affected by a
618 colliding anticyclonic ring. *Journal of Oceanography*, *50*, 559-588.
- 619 Vukovich, F. M. (2007, March). Climatology of Ocean Features in the Gulf of Mex-
620 ico Using Satellite Remote Sensing Data. *Journal of Physical Oceanography*,
621 *37*(3), 689-707. doi: 10.1175/JPO2989.1
- 622 Watts, D. R., Sun, C., & Rintoul, S. (2001, August). A Two-Dimensional Gravest
623 Empirical Mode Determined from Hydrographic Observations in the Sub-
624 antarctic Front. *Journal of Physical Oceanography*, *31*(8), 2186-2209. doi:
625 10.1175/1520-0485(2001)031<2186:ATDGEM>2.0.CO;2
- 626 Wilder, T., Zhai, X., Munday, D., & Joshi, M. (2022). The response of a baroclinic
627 anticyclonic eddy to relative wind stress forcing. *Journal of Physical Oceanog-
628 raphy*.